EUROPEAN FUSION DEVELOPMENT AGREEMENT

EFDA–JET–PR(06)01

D.C. McDonald, J.G. Cordey, K. Thomsen, O.J.W. F. Kardaun, J.A. Snipes, M. Greenwald, L. Sugiyama, F. Ryter, A. Kus, J. Stober, J.C. DeBoo, C.C. Petty, G. Bracco, M. Romanelli, Z. Cui, Y. Liu, Y. Miura, K. Shinohara, K.Tsuzuki, Y. Kamada, T. Takizuka, H. Urano, M. Valovic, R. Akers, C. Brickley, A. Sykes, M.J. Walsh, S.M. Kaye, C. Bush, D. Hogewei, Y. R. Martin, A. Cote, G. Pacher, J. Ongena, F. Imbeaux, G.T. Hoang, S. Lebedev, A. Chudnovskiy, V. Leonov and JET EFDA contributors*

Recent Progress on the Development and Analysis of the ITPA Global H-Mode Confinement Database

Recent Progress on the Development and Analysis of the ITPA Global H-Mode Confinement Database

D.C. McDonald[1], J.G. Cordey[1], K. Thomsen[2], O.J.W. F. Kardaun[2], J.A. Snipes[3], M. Greenwald[3], L. Sugiyama[3], F. Ryter[4], A. Kus[4], J. Stober[4], J.C. DeBoo[5], C.C. Petty[5], G. Bracco[6], M. Romanelli[6], Z. Cui[7], Y. Liu[7], Y. Miura[8], K. Shinohara[8], K.Tsuzuki[8], Y. Kamada[8], T. Takizuka[8], H. Urano[8], M. Valovic[1], R. Akers[1], C. Brickley[1], A. Sykes[1], M.J. Walsh[1], S.M. Kaye[9], C. Bush[9], D. Hogewei[10], Y. R. Martin[11], A. Cote[12], G. Pacher[12], J. Ongena[13], F. Imbeaux[14], G.T. Hoang[14], S. Lebedev[15], A. Chudnovskiy[16], V. Leonov[16] and JET EFDA contributors*

[1]*EURATOM/UKAEA Fusion Association, Culham Science Centre, Abingdon, Oxon, OX14 3DB, UK*
[2]EFDA Close Support Unit, D-85740 Garching, Germany
[3]*MIT Plasma Science and Fusion Center, Cambridge, MA, USA.*
[4]*Max-Planck Inst. für Plasmaphysik, Garching*
[5]*General Atomics, San Diego, CA, USA*
[6]*Associazione Euratom-ENEA sulla fusione, Frascati, Italy*
[7]*South Western Institute of Physics, Chengdu, China*
[8]*Naka Fusion Research Establishment, Japan Atomic Energy Research Institute, Naka-machi, Naka-gun, Ibaraki-ken, Japan.*
[9]*Princeton Plasma Physics Laboratory, Princeton, NJ. USA*
[10]*FOM Instituut voor Plasmafisica, Rijnhuizen, Nieuwegein, The Netherlands*
[11]*EPFL/CRPP Association Euratom, Lausanne, Switzerland*
[12]*Centre Canadien de Fusion Magnetique, Varennes, Québec, Canada*
[13]*LPP/ERM-KMS, Association EURATOM-Belgium State, Brussels, Belgium*
[14]*Association EURATOM-CEA, CEA/DSM/DRFC, CEA Cadarache, Saint-Paul lez Durance, France*
[15]*A.F. Ioffe Institute, Russian Academy of Sciences, St. Petersburg, Russia*
[16]Nuclear Fusion Institute, Russian Research Centre Kurchatov Institute, Moscow, Russia
** See annex of J. Pamela et al, "Overview of JET Results ", (Proc. 20th IAEA Fusion Energy Conference, Vilamoura, Portugal (2004)).*

Preprint of Paper to be submitted for publication in
Nuclear Fusion

ABSTRACT

This paper describes the updates to and analysis of the International Tokamak Physics Activity (ITPA) Global H-Mode Confinement Database version 3 (DB3) over the period 1994 – 2004. Data have now been collected from 18 machines of different sizes and shapes: ASDEX, ASDEX Upgrade, C-Mod, COMPASS-D, DIII-D, JET, JFT-2M, JT-60U, MAST, NSTX, PBX-M, PDX, START, T-10, TCV, TdeV, TFTR, and TUMAN-3M. The database now contains data from deuterium-tritium experiments, low aspect ratio plasmas, dimensionless parameter experiments and helium-4 plasmas. DB3 also contains an increased amount of data from a range of diverted machines and further data at high triangularity, high density and high current. A wide range of physics studies has been performed on DB3 with particular progress made in the separation of core and edge behaviour, dimensionless parameter analyses, and the comparison of the database with one-dimensional transport codes. The errors in the physics variables of the database have also been studied and this has led to the use of Errors in Variables fits. A key aim of the database has always been to provide a basis for estimating the energy confinement properties of next step machines such as ITER, and so the impact of the database and its analysis on such machines is also discussed.

1 INTRODUCTION

This paper reviews the work of the International Tokamak Physics Activity (ITPA) H-mode Database Working Group (formerly the ITER H-Mode Database Working Group) on the scaling of energy confinement in H-mode tokamak plasmas over the period 1994 to 2004. This covers the construction of the ITPA Global H-Mode Confinement Database version 3 (DB3) and the physical interpretation of this database. This work has involved collaboration between teams at ASDEX Upgrade, C-Mod, COMPASS-D, DIII-D, JET, JT-60U, MAST, NSTX, START, T-10, TCV, TdeV, TFTR, and TUMAN-3M.

The first version of the H-Mode Database was released as ITERHDB.1 (DB1) in 1992 [1] and succeeded by ITERHDB.2 (DB2) in 1994 [2]. DB3 is an extension of DB2 and contains almost twice as many data, as well as almost 50% more variables. Major additions to DB3 include

1. Data from 12 additional machines and further data from JET and DIII-D.
2. Data from low aspect ratio devices (MAST, NSTX, and START).

3. Data from tritium and deuterium-tritium plasmas (JET and TFTR) including discharges with fusion product in excess of 0.6.
4. Data from dimensionless parameter identity experiments and individual dimensionless parameter scans (ASDEX Upgrade, C-Mod, COMPASS-D, DIII-D, JET, JT-60U, and TFTR.)
5. Data from helium-4 discharges (DIII-D and JET.)
6. Increased data from discharges with plasma currents in excess of 4 MA.
7. A significant increase in data from experiments at triangularity of 0.35 or above (ASDEX Upgrade, C-Mod, COMPASS-D, DIII-D, JET, JT-60U, TCV, START, MAST and NSTX)
8. The addition of new variables describing ELM behaviour, divertor type, pellet and gas fuelling, impurity injection, upper and lower triangularity, alpha-heating, and q-profile shear.

Analysis of the database has focused on both the improvement of the physics models used to describe the data and the improvement of the statistical methods used to fit the physical models to the data. Some of the main areas covered by the physics analysis of energy confinement using DB3 were the separation of the core and edge confinement, the impact of plasma shape, dimensionless parameter studies, the impact of fuelling, and comparisons of the database with one dimensional transport models. Statistical analyses concentrated on understanding and reducing the correlations in the dataset, estimation of the errors in the database variables, the use of Errors in Variables (EIV) methods, and improved techniques for estimating confidence intervals for ITER.

As well as reviewing the work done in all of the above areas, this paper also contains detailed descriptions of the data added since DB2, a new analysis of the global pedestal database with a resulting two-term scaling, and a set of recommended scalings for extrapolating results to ITER and next step machines.

The rest of this paper is structured as follows: Section 2 describes the improvements and additions to the data that each tokamak has made. Section 3 describes the standard ELMy H-mode datasets derived from DB3 and their condition with respect to the variables commonly

used in fits to them. Section 4 then discusses power law fits to the standard global energy confinement datasets. Section 5 describes fits to the pedestal-global confinement dataset which have produced two-term global energy confinement scalings. Section 6 describes how the resulting fits are extrapolated, with the emphasis on next step devices such as ITER. Finally, section 7 draws the results together and indicates the recommended scalings and shows how they are applied to ITER.

2 CHANGES AND ADDITIONS TO THE H-MODE ENERGY CONFINEMENT DATABASE

In addition to the 6 machines which contributed data to DB2 [2], an additional 12 machines: ASDEX Upgrade, C-Mod, COMPASS-D, JT-60U, MAST, NSTX, START, T-10, TCV, TdeV, TFTR, and TUMAN-3M; have contributed data to DB3. Furthermore, JET and DIII-D, who contributed data to DB2, have also continued to supply new data to DB3. One further discharge has also been added by JFT-2M, but this does not significantly alter the description of the data from Ref. 2. With the exception of JFT-2M, then, the details of the data supplied by each tokamak, together with a brief overview of how they were produced, are given in Sections 2.1 - 2.14. These sections also describe the data included in the International Pedestal Database, which is relevant to Section 5.

DB2 contained 111 variables which has now been extended to 164 for DB3. These additional variables are listed in Appendix A, along with the two variables which have been renamed. As with DB1 and DB2, the time traces of key parameters in the discharges of DB3 are given in the form of review sheets and are also discussed in Appendix A.

For each machine, the equilibrium is reconstructed from magnetics data, with in some cases additional constraints from other diagnostics, to give the poloidal flux, ψ, as a function of major radius, $\boldsymbol{R}$, and vertical height, $\boldsymbol{Z}$. By convention, ψ is normalised to be 0 at the magnetic axis and 1 at the last closed flux surface. From this equilibrium the following quantities can then be derived: the plasma minor radius, $\boldsymbol{a}$, major radius, $\boldsymbol{R}$, inverse aspect ratio, $\varepsilon = \boldsymbol{a}/\boldsymbol{R}$, elongation, κ, triangularity, δ, cross-sectional area, $\boldsymbol{A}$, surface area, $\boldsymbol{S}$, and volume, $\boldsymbol{V}$, toroidal magnetic field, $\boldsymbol{B}$, plasma current, $\boldsymbol{I}$, q-profile, $\boldsymbol{q}$, and internal inductance, $\boldsymbol{l}_i$, defined as the ratio of the mean of the squared poloidal magnetic field to its value at the last closed flux surface. Additional

plasma diagnostics measure the electron density, n_e, electron (ion) temperature, $T_{e(i)}$, Z-effective, Z_{eff}, plasma rotation, v_{rot}, effective isotope mass, M, and radiated power, P_{RAD}. The total plasma energy, W, can be taken as the integral of the kinetic measures, W_{KIN}, or, from the MHD energy, W_{MHD}, or the diamagnetic energy, W_{DIA}. If W_{MHD} or W_{DIA} are used, the effects of the energy in the fast, non-thermal, particles, W_{FAST}, must be calculated and removed. Combined with the loss power across the last closed flux surface, P, this enables the calculation of the energy confinement time, $\tau_E = W/P$. Other key parameters, which can be derived from those quoted so far, are the line average electron density, n, poloidal beta, β_p, normalised toroidal beta, β_N, and q_{95}, the value of q at $\psi = 0.95$.

For the pedestal-global confinement dataset, a subset of data from the ITPA pedestal database [3] is used. The combined dataset comprises only the discharges and time points in the pedestal database that also appear in the global confinement database. These 453 entries represent a small subset of the 10263 entries in the complete pedestal database. For the machines that contribute to this subset, brief descriptions of how the data relating to the pedestal energy, W_{ped}, was calculated are given.

2.1 ASDEX Upgrade

ASDEX Upgrade (AUG) is a medium size divertor tokamak with capabilities for plasma shaping. Its major radius is 1.65 m and minor radius is 0.50 m. The plasmas are D-shaped with typical plasma elongation of about 1.6 and averaged upper and lower triangularity between 0.15 and 0.4. The toroidal magnetic field has been operated from 1 T to 3.4 T and the plasma current between 0.4 and 1.4 MA. The electron line average density ranges from about 1.0 _ 10^{19}.m^{-3} to 15 _ 10^{19}.m^{-3}. The main auxiliary heating method is provided by NBI (D or H) up to 20 MW. Further heating methods are ICRF up to 3.5 MW in plasma (generally hydrogen minority in deuterium) and ECH (2nd harmonic X-mode) up to 1.6 MW. The first wall and divertor are composed of carbon tiles with different coatings (boronisation, siliconisation and partially tungsten during some periods) as indicated in the database. The divertor geometry has been modified with time, as indicated in the corresponding variable, keeping in all cases an effective

baffling of neutrals. As a result, H-modes are easily obtained with power levels much lower than the full available heating power.

The main set of diagnostics in ASDEX Upgrade providing the measurements for this database are: Electron Cyclotron Emission (ECE) and Thomson scattering for measuring $T_e(\psi,t)$; DCN interferometry for core and Li-beam for edge density measurement providing density profiles $n_e(\psi,t)$ by a combined deconvolution; Thomson scattering and reflectometry for further $n_e(\psi,t)$ data; Toroidal and poloidal arrays of the CXRS diagnostic deliver $T_i(\psi,t)$ and $v_{rot}(\psi,t)$ in NBI heated plasmas; For Ohmically heated plasmas neutral particle analyses provide $T_i(\psi,t)$, as well as the H/D ratio; A visible Bremsstrahlung array for measuring $Z_{eff}(\psi,t)$; Bolometer arrays for measuring radiated power profiles, $P_{RAD}(\psi,t)$ of main and divertor plasmas; Various spectrometers for determining impurity content; A full set of magnetic diagnostics for calculating the MHD equilibrium and related quantities. The plasma-stored energy is calculated by integration of the density and temperature profiles (WKIN) and by analysis of the equilibrium with the equilibrium code (WMHD). The stored energy is also obtained from analysis of the diamagnetic loop signals. These are in good agreement with WMHD.

The shots for confinement analysis included in this database were chosen to be in quasi-steady state with respect to stored energy, density, and magnetic equilibrium. The plasma parameters cover the range attainable in the machine. Hydrogen and deuterium plasmas are included. The heating powers are estimated by the appropriate deposition codes or by approximated fit formulae. In this dataset, the majority of the shots were heated with NBI. The confinement data are generally time-averaged over sawteeth and ELMs but are not taken during other MHD events degrading confinement such as neoclassical tearing modes. Restrictions concerning excessively high radiative power or dW/dt are applied in the selection criteria.

The ASDEX Upgrade contribution to the pedestal database has evolved over time with the development of better edge diagnostics. The older pedestal-top data are based on measurements from the core Thomson scattering system. Electron temperatures and densities from 2 cm inside the nominal separatrix position were provided. More recently (for shots since approximately 1999), data are provided as the upper level of a modified hyperbolic tangent fit to the edge profile, based largely on data from the edge Thomson scattering system. Data are provided both averaged over ELM cycles and synchronized to short periods just before or after ELM crashes.

For the study of data combined between the pedestal and global databases, the ELM averaged data were used. As there is not yet an edge CXRS system on ASDEX Upgrade, it is recommended to approximate the total pedestal-top pressure by doubling the electron pressure.

2.2 C-Mod

C-Mod is a compact high-field tokamak with a closed divertor and with capabilities for strong plasma shaping. Its major radius is 0.68 m, minor radius is 0.22 and the toroidal field has been operated from 2.4 to 8.0 T. The plasma current for these studies ranged from approximately 0.24 to 1.2 MA. Typical plasma elongations are in the range 1.58 - 1.8. The plasmas are D shaped, though the divertor geometry is best utilized with lower triangularity values in the range 0.5 - 0.6. Upper triangularity is typically 0.3 - 0.4 yielding an average triangularity near 0.4. A few discharges in the database have higher average triangularity, ranging up to 0.7. The plasma line average density ranged from 1.3 to 4.3 _ 10^{20}.m^{-3}, with the better H-modes all above 2 _ 10^{20}.m^{-3}. The auxiliary heating method is ICRF; employing hydrogen minority in deuterium plasmas at $\boldsymbol{B}$ = 5.3 T as the principal scenario. For experiments in the database, up to 3.5 MW of RF power was available. Because of the large $\boldsymbol{B/R}$ ratio in C-Mod, Ohmic heating is never negligible, contributing 0.4 - 1.1 MW in H-mode, depending on plasma temperature and purity. The first wall is composed of molybdenum tiles and is designed to take the very high power loadings which occur in this experiment; values for the parallel heat flux up to 0.5 GW.m^{-2} have been measured. The C-Mod divertor geometry, combined with the high densities, results in very effective baffling of neutrals. Divertor compression, the ratio of neutral pressure in the divertor chamber to the pressure in main plasma chamber, ranges from 100 to 300.

H-modes are easily obtained in C-Mod with Ohmic and RF heating, over a wide range of L-mode target conditions including densities up to 3 _ 10^{20}.m^{-3} and fields up to 8T [4]. The power required for the L-H transition is consistent with $\boldsymbol{P_{TOT}/S = 0.02 - 0.04 \cdot nB}$; with $\boldsymbol{P_{TOT}}$ measured in MW, $\boldsymbol{S}$ in m^2, $\boldsymbol{n}$ in 10^{20}.m^{-3} and $\boldsymbol{B}$ in T. The factors that cause the variation in required input power are not well understood, but seem to be related to impurity levels, wall conditioning, and neutral pressure. Initially, the H-modes were characterized by strong, high frequency, type III ELMs or brief ELM-free periods with accumulating impurities and high ratios of $\boldsymbol{f_{RAD} = P_{RAD}/P_{TOT}}$. These results, combined with those reported on other devices, have led to the study of the effect of boronizing the vacuum chamber. In C-Mod, vessel conditioning

is accomplished via electron cyclotron discharge cleaning, ECDC, in which 2.5 kW of microwave power at 2.45 GHz are applied as the toroidal field is slowly ramped from 0.06 to 0.14 T (measured at R = 0.67 m), sweeping the resonance over the vacuum wall. For boronisation, the discharge cleaning gas was replaced with a 9:1 mixture of He and diborane (B_2D_6). The boron coating was renewed about once a week. Following boronisation, radiated power, which was primarily due to molybdenum, was lower and H-mode performance was dramatically improved.

The C-Mod data include those taken from ELM free shots and from a new regime [5], which is characterized by good energy confinement, moderate particle confinement, and no large, type I ELMs. The pedestal electron temperature can reach 600-800 eV, well above the measured threshold for type III ELMs, and the pressure gradient in the transport barrier is near or above first stability ideal MHD limits. This regime has been named the EDA or Enhanced D_α H-mode after its salient characteristic. While energy confinement in the EDA regime is only about 10% below that found in ELM free discharges, the impurity particle transport is much lower with no impurity accumulation, resulting in much lower radiated power. EDA discharges can last, without obvious change, for the duration of the RF heating pulse, about 10 energy confinement times so far. Unlike standard ELMy discharges, which undergo periodic relaxation oscillations, EDA plasmas show no significant intermittent loss of energy and particles, though small inconsequential ELMs are sometimes superimposed when $\beta_N > 1.2$. The edge gradients seem to be limited by a continuous process associated with a short wavelength quasi-coherent mode which has been observed with electrostatic and magnetic probes, as well as phase contrast imaging, reflectometry, BES and optical imaging.

The set of diagnostics available for transport studies on C-Mod includes ECE and Thomson scattering for measuring $T_e(\psi,t)$; a two-colour interferometer (TCI), reflectometry, and Thomson scattering for determining $n_e(\psi,t)$; an array of high resolution X-ray spectrometers for measuring $T_i(\psi,t)$; neutron emission diagnostics for determining $T_i(0,t)$; a visible bremsstrahlung array for measuring $Z_{eff}(\psi,t)$; a bolometer array for measuring radiated power profiles, $P_{RAD}(\psi,t)$; various spectrometers for determining impurity content; and a full set of magnetic diagnostics for calculating the MHD equilibrium and related quantities. The plasma stored energy is calculated by integration of the density and temperature profiles (W_{KIN}) and by analysis of the equilibrium with the EFIT code (W_{MHD}). These generally agree to within 20%.

Most of this discrepancy can be understood as the result of errors in experimentally measured quantities; A residual systematic difference between the magnetic and kinetic calculations remains. The larger part of this difference can be explained as kinetic energy stored in the minority ion tail, leaving a residual systematic difference about 5-10% of the total. Shots for confinement analysis were chosen to be in quasi-steady state with respect to stored energy, density, and magnetic equilibrium. Time slices used for comparison with scaling laws were chosen with $f_{RAD} < 0.5$; $dW/dt < 0.35 \cdot P_{IN}$; $dn_e/dt < 0.4 \cdot n_e/\tau_E$; and $q_{95} > 3$. For full profile and time-dependent analysis the TRANSP code is used. This code uses measured plasma profiles as inputs then calculates the electron and ion heat balance, particle balance, and magnetic diffusion with a fixed boundary equilibrium. For ICRF heated plasmas, the full wave SPRUCE or TORIC codes linked to the Fokker-Planck solver FPPRF was used to calculate the heating power to ions and electrons. These codes assume perfect wave power absorption, and thus overestimate absorbed power. From transient analysis of RF perturbations, the absorbed fraction has been estimated to be 90% ± 10% and this number is used for all global calculations in the database. For C-Mod H-modes, which are at high densities, code results indicate that the energy in fast ions is less than 5%. The thermal nature of these plasmas is confirmed by observation of sawtooth reheat rates, which show very little contribution to plasma heating from fast ions immediately following the turn-off of ICRF power. For similar reasons, the electron and ion temperatures are not very different. The ion-electron equilibration time, τ_{ei}, ranges from 2 ms near the plasma edge to 10 ms in the core. These values are much less than the energy confinement time.

Pedestal data are available for only a subset of H-mode confinement points. Most were EDA, while a few ELM-free discharges were included. A range of input powers were used, and, in contrast to type I ELMy H-modes, it is likely that pedestal gradients were below MHD stability limits. The source and accuracy of these data varies according to the diagnostics available at the time of experiments. Early edge data supplied to the pedestal database from 1996 experiments were for the purpose of mapping out edge operational spaces, including L-H transitions and various ELM types, and in general do not correspond to the points used for H-mode confinement analysis. For data prior to 1999, pedestal temperatures are measured using the core ECE diagnostic described above. A standard location at poloidal flux surface $\psi = 0.95$ was used for the 1996 dataset. For 1998 experiments, a set of discharges used for confinement studies was analysed and an average value in the radial region between poloidal flux surfaces $\psi = 0.85$ and

$\psi = 0.95$ was used; detailed measurements using $\boldsymbol{B}$ sweeps have found this to be the region in which the edge $\boldsymbol{T_e}$ gradient begins to deviate from that of the core [4]. Uncertainties in $\boldsymbol{T_{e,ped}}$ are estimated to be ± 10%. No edge density measurements were available during this period; pedestal densities were estimated as 65% of line average density and have relatively large uncertainties (≈ ± 20%). Pedestal stored energies $\boldsymbol{W_{e,ped}}$ and $\boldsymbol{W_{ped}}$ were computed using the total plasma volume (an overestimate) and assuming equal ion and electron contributions.

Since 1999 the study of the H-mode pedestal on C-Mod has been aided by an edge Thomson scattering (ETS) diagnostic with high spatial resolution [5]. The ETS system measures $\boldsymbol{T_e}$ and $\boldsymbol{n_e}$ at the upper edge of the plasma at $\boldsymbol{R}$=69 cm, obtaining profiles with a nominal radial resolution of 1.3mm after mapping to the midplane along flux surfaces reconstructed by EFIT. The dynamic range of the ETS diagnostic is approximately 20—800 eV, 3_10^{19}—5_10^{20}.m^{-3}, which encompasses conditions throughout the H-mode pedestal region in most operational regimes. A dramatic increase in $\boldsymbol{T_e}$ and $\boldsymbol{n_e}$ gradients is observed in the ETB region upon transition from L to H-mode. Gradient scale lengths of millimetres are typical in C-Mod pedestal profiles. An interesting feature in the $\boldsymbol{T_e}$ profile, observed in a number of steady H-mode discharges, is a region of $\boldsymbol{T_e}$ gradient intermediate between that in the pedestal (50-100 keV.m^{-1}, typically) and that in the core plasma (5-10 keV.m^{-1}). This region is located immediately inside the $\boldsymbol{T_e}$ pedestal and is approximately 1cm in radial extent. The change in $\boldsymbol{T_e}$ gradient in this region has been observed with both ECE and ETS, though the adjacent pedestal seen with ETS is too localized to be measured with ECE [6]. Unfortunately the radial extent of the transition region between pedestal and core is not routinely diagnosed, and not well characterized at this time. The outer ETB profiles, however, are regularly measured with ETS.

More detailed pedestal data, obtained primarily from the ETS diagnostic, were submitted to the pedestal database for selected EDA H-mode discharges dating after 1999 from the global database; these have been merged with the global confinement database and only the time windows with entries in both tables are used in two-parameter fits. H-mode pedestal profiles are averaged over the steady period of the discharge and fit with a standard parameterized function [7]. A convenient set of fitting parameters [$\boldsymbol{b}$ (baseline), $\boldsymbol{h}$ (height), $\boldsymbol{R}_0$ (position), Δ (full width) and $\boldsymbol{m}$ (interior slope)] are obtained from this function, defined on midplane radius $\boldsymbol{R}$:

$$f(R) = b + \frac{h}{2}\left[\tanh\left(\frac{R_0 - R}{d}\right) + 1\right] + m(R_0 - R - d)H(R_0 - R - d), \qquad (1)$$

where $H(x)$ is a Heaviside function, and $d = \Delta/2$ is the pedestal half-width. At the base of the pedestal ($R = R_0 + d$), $f \approx b$; the value of f atop the pedestal ($R = R_0 - d$), is approximately $b + h$. The variables TEPED, NEPED and PEPED correspond to this location at the top of the steep barrier region, which is typically at $\psi \approx 0.97$, somewhat outside the location used in earlier data and therefore having lower temperatures. Statistical errors in the fitted values are typically <5 %, though systematic uncertainties in pedestal density are estimated at ≈15%. Pedestal stored energy was computed based on PEPED, taking the volume at the midpoint of the pressure pedestal, typically 2-4 mm inside the LCFS. A complete set of pedestal fit parameters are contained in the pedestal database. Additional variables NEEDGE, TEEDGE were also supplied, taking data at a position corresponding to the inner break-in-slope as described above. The question of which location sets the most relevant 'boundary condition' for global confinement is a general and currently open one.

Systematic studies over a wider C-Mod dataset have shown that most pedestal widths are in the range of 2-6 mm ($\Delta/a \approx 1-3\%$), with width seen in the temperature profile slightly larger, on average, than that seen in the density profile [8]. Pedestal widths do not respond systematically to changes in global plasma parameters, such as toroidal field and current and exhibit a high degree of scatter, dominated by random profile fluctuations. Varying plasma shape has been shown to systematically affect pedestal width and other ETB properties. The feet of the T_e and n_e pedestals, where the respective profile values tend toward b_T and b_n, both exist near the LCFS, and the baseline values typically measure 15-30 eV and 3-5x10^{19}.m^{-3}. This puts the foot of the pedestal in the near SOL, since power balance requires T_e between 50 and 100 eV at the LCFS of almost all C-Mod plasmas. Pedestals exhibit a wide range of peak values (n_e: 1-5x10^{20}.m^{-3}, T_e: 200-1000 eV) and characteristic gradients, and are sensitive to a number of operational parameters.

2.3 COMPASS-D

COMPASS-D is a research tokamak with major and minor radii 0.56 m and ≈ 0.17 m respectively. It has a flexible plasma shaping system although the data exported to the database are restricted to single null divertor plasmas. Shapes with relevant elongation ≈ 1.7 and high triangularity ≈ 0.4 are represented in particular.

Predominantly deuterium is used as a working gas although experiments with hydrogen and helium have been conducted as well. Regular boronisation is applied to treat the walls. The divertor is open with graphite tiles as the plasma facing material. Glow discharge cleaning in helium is used before each shot.

COMPASS-D is equipped with an ECRH system (60 GHz, < 1.5 MW). H-mode has been obtained with both fundamental and second harmonic resonance heating. The ELMy H-mode has been produced so far only at fundamental resonance. In this regime the waves are launched from up to 5 high field side antennas with X-mode polarisation and oblique propagation relative to the major radius. For shots in the database the launching angles are balanced, as far as possible, so that no significant current drive is expected.

The energy content is determined from the diamagnetic signal and equilibrium reconstruction (EFIT). Electron temperature and density profiles are measured by Thomson scattering. The ion temperature is measured by a neutral particle analyser. The ECRH absorption is calculated using ray-tracing/Fokker-Plank code BANDIT-3D. The plasma cross-sectional area for COMPASS-D discharges was not submitted to DB3. Where required, it should be approximated by $A \approx V/(2\pi R)$.

COMPASS-D routinely operates in stationary ELMy H-mode with Ohmic heating. The operational window is controlled by plasma density. Ohmic heating allows a large range of q-values. Operation down to q_{95} = 2.6 was possible without significant deterioration of confinement.

A unique feature in COMPASS-D is operation in stationary ELMy H-mode with on-axis ECRH. The operational window is determined simultaneously by density and power thresholds [9]. Line average densities above $n \approx 3.6 \times 10^{19}$.m^{-3} and launched power greater than $P_{ECRH} \approx 0.5$ MW are required. In order to achieve a regime with well-separated ELMs increased triangularity seems necessary. These regimes can last for the whole duration of the heating pulse. With decreasing plasma current the ELM frequency decreases.

A factor of four range in normalised collisionality, ν^*, is possible by matching an ECRH shot with an Ohmically heated plasma. These plasmas, dominated by electron heat transport, showed a weak dependence of global confinement on collisionality [10].

2.4 DIII-D

DIII-D has been contributing data to the H-mode confinement database since its inception. Contributions to the prior version of the database, DB2, were described in Ref. 11 and 2. The new DIII-D contributions to DB3 include 226 discharges with a total of 271 time slices which include both ELMy and ELM-free H-mode phases. Contributions to DB2 included some operation with carbonized walls. For the new data contributed to DB3 some additional carbonized wall operation is included but most contributions are with boronised walls which has become the preferred process for wall preparation on DIII-D. Comparison of the two types of preparation can be identified with the EVAP database parameter. Boronisation has led to further reduction of oxygen compared to carbonisation and also results in a reduction of high-Z metals [12]. Impurity control with boronisation lasted longer than carbonisation before a fresh application was required. Carbon from the carbon tiles covering the vacuum vessel walls is the dominant contributor to Z_{eff}.

The main diagnostic set used to provide DIII-D data to the database includes a Thomson scattering system for $T_e(\psi,t)$ with 44 spatial measurements in both the main plasma and divertor region, a charge exchange recombination system with 40 spatial measurements for $T_i(\psi,t)$, toroidal and poloidal rotation velocity profiles and Z_{eff} profiles through measurement of the carbon density profile, a 40 channel ECE diagnostic for $T_e(\psi,t)$ and a 4 chord CO_2 interferometer system for line average density measurements. The radiated power profile is determined with two arrays of bolometers, each with 24 channels. A complete set of magnetic diagnostics is used along with the EFIT code [13,14] to reconstruct the plasma equilibrium flux and convert diagnostic measurements from (R,Z)coordinates to a flux coordinate system that allows measurements made at different R and Z locations to be combined together to compute a composite profile in flux coordinates. The plasma stored energy is determined from the equilibrium reconstruction or from integration of the profiles to provide WMHD or WKIN respectively.

H-modes created with neutral beam heating, electron cyclotron heating and ion cyclotron heating are included in this dataset showing that the L- to H- mode transition is not dependent upon a specific type of heating power. Global data from discharges that were originally contributed to the profile database (containing detailed profile information and used primarily to compare measured profiles with simulations based on various transport models) is included in the new DIII-D dataset.

Additional data are included from two specific areas of study, dimensionless parameter scaling studies and confinement at high density. The scalings of heat transport with normalized gyroradius [15], beta [16], and collisionality [17] – see Section 4.3 for definitions – have been individually measured and the global parameters from these discharges are included in the H-mode database. The results of these studies provide constraints on theoretical models of turbulent transport in DIII-D. Generally the results indicate that, for low q H-mode discharges, global confinement scales as gyro-Bohm-like which is consistent with many of the theories that assume the radial correlation length scales with the Larmor radius. Only a weak scaling with β is observed which favours electrostatic over electromagnetic loss mechanisms. A moderate scaling with collisionality is observed which falls between the dependencies of trapped electron and ITG modes and resistive ballooning modes. Other scaling studies with q, T_e/T_i and κ have been performed on DIII-D and have been added to the latest, working version of the H-mode database.

DIII-D has demonstrated that it is possible to obtain good confinement at high density transiently with pellet injection [18] and in closer to steady state conditions with gas puffing [19,20]. Examples of both types of fuelling are included in the database. ELMing H-mode discharges with densities up to 40% above the Greenwald density limit, fuelled by deuterium gas puffing, were obtained with good energy confinement times, $H_{98P} = 2$. These discharges had performance levels comparable to the best pellet fuelled discharges. Simultaneous gas fuelling and divertor pumping were required. Spontaneous peaking in the density profile played a key role in obtaining high energy confinement times.

DIII-D also contributes data to the ITPA pedestal database and for those discharges common to both that database and the global H-mode database described in this paper the values of pedestal stored energy were used to study two-term global confinement time scaling expressions. The DIII-D data in those studies were predominantly from single-null divertor discharges with ELMs. The electron and ion pressure profiles, averaged over ELMs, were individually determined from the profile diagnostics and then the edge region of each profile was fit to a

TANH function [21] to determine the electron and ion pedestal pressure. The electron and ion pedestal stored energy was then determined from the pedestal pressure.

2.5 JET

The 1587 JET data entries DB2 [2] cover the period following the 1992-4 shutdown until the end of 2002. In this period JET began divertor operation, studying three different designs in total; performed deuterium-tritium experiments which set world records for fusion power and energy; and has recently concentrated on high density, high performance, steady state H-mode discharges with edge behaviour and impurity transport that scale to acceptable levels for next step devices. JET DB2 data tended to have multiple time slices, but the new data are almost exclusively taken from one time point per shot, except for shots where parameters are varied.

Since 1994, JET has operated with diverted plasmas, beginning with the relatively open Mk I [22] and moving to the more closed Mk IIA [23], Mk IIAP [23] and the gas box Mk IIGB [24] designs. This has resulted in steady state ELMy H-modes, in contrast to the pre-1994 undiverted plasmas of DB2 which tended to be transient. JET DB3 data covers a wide range of configurations, with different divertor flux expansions [23], elongation [25] and triangularity [26,27]. Discharges are mostly deuterium gas fuelled, heated with Neutral Beam Injection (NBI) and/or Ion Cyclotron Resonant Heating (ICRH). As for the DB2 shots, regular beryllium evaporations and glow discharges have proved vital for reducing impurity levels.

Tritium and deuterium-tritium operation in 1997 [28] provided DB3 with data for type I and type III ELMy, as well as ELM free, H-modes. These include shots with α-heating up to 2.8 MW and fusion gain, $\boldsymbol{Q}$, of 0.62. Steady state discharges with $\boldsymbol{Q} > 0.2$ are also included. Together with further deuterium, hydrogen and helium-4 discharges, JET has contributed a wide range of isotope data [29,26,30]. High confinement (HIPB98(y,2) $\approx$ 1) type I discharges have been achieved at densities approaching and exceeding the Greenwald density limit [31] using high triangularity [26,27], pellet injection [32] and density peaking [33,24]. DB3 also contains data from type III ELMy H-mode studies [34], hot ion H-modes [35] and the combined type I-II ELMy H-modes [27]. Impurity seeding has been used to moderate divertor power loads [36,27]. Experiments based on non-dimensional transport scaling [37,38], have included ITER "wind tunnel" experiments ($\rho*$ scans at fixed β and $\nu*$) with DIII-D [39]; $\rho*$, β, and $\nu*$ scans [40,41,42]; and identity experiments with ASDEX Upgrade, C-Mod and DIII-D [43, 44].

A new ICRH system of 4 antennae each with 4 current straps was installed in 1994. The system allows quadrupole phasing as well as the monopole and dipole permitted in the old system. Fundamental and 2nd harmonic hydrogen, helium-3 and 2nd harmonic tritium minority heating schemes [45] are all represented in the new data. Combined heating shots, including dedicated experiments varying the ratio of ICRH/NBI [46,47], are also included. The neutral beam system remained largely as in DB2, but with a vertical steering facility to ensure central power deposition in raised plasma configurations. DB3 contains shots heated with hydrogen, deuterium and tritium beams.

$n_e(\psi,t)$ measurements are provided by an 8 channel interferometry system and a LIDAR Thomson Scattering system. $Z_{eff}(\psi,t)$ is measured by Charge Exchange Spectroscopy or, where this is not available, by visible spectroscopy of bremsstrahlung radiation on one chord and assuming spatial inhomogeneity. The fractional concentration of hydrogenic and helium species are also measured with visible spectroscopy. $T_e(\psi,t)$ measurements are taken from the LIDAR Thomson Scattering system. $T_i(\psi,t)$ is measured with Charge Exchange Spectroscopy or, when this is not available, by taking $T_i(t)$ from an X-ray crystal spectrometer and assuming the ratio T_i/T_e is constant across the plasma. $P_{RAD}(\psi,t)$ is measured with a bolometry system and neutron emissions using neutron yield monitors. Equilibria are reconstructed using the EFIT code based on data from magnetic coils. Fast particle energies are calculated from the PENCIL and PION codes – or a fitted formula otherwise - and removed from the diamagnetic energy measurement to give the plasma thermal energy.

JET has also contributed data to the ITPA global pedestal database, of which 161 entries are common to the global confinement database. These span the period 1997-2001 during Mk IIa and Mk IIGB divertor operation. They include type I and type III ELMy H-modes with a variety of elongations and triangularities and both NBI and ICR heating. Hydrogen, deuterium and deuterium-tritium discharges are included. The method used to determine the pedestal density and ion and electron temperatures is given in Reference 26. An ECE diagnostic is used to identify the top of the pedestal, ψ_{ped}, and to measure $T_e(\psi_{ped},t)$. $T_i(\psi_{ped},t)$ is then measured with Charge Exchange Spectroscopy and $n_e(\psi_{ped},t)$ with interferometry. The resulting pressure profile is integrated to give the pedestal energy. In general, diagnostic spatial resolution does not resolve the pedestal structure and so a fixed width and gradient is assumed. Because of the cut-

off properties of the waves used by the JET ECE system, the edge electron temperature of plasmas with $B < 1.7$ T cannot be measured and so do not appear in the JET pedestal dataset.

2.6 JT-60U

JT-60U data for shots 22110 and 22111 are the result of high-density ELMy H-mode experiments [48]. These discharges maintain the standard level of confinement in JT-60U before the start of degradation due to high density. Data for shots 23555-27390 are the result of non-dimensional transport experiments [49]. The dependence of ELMy H-mode transport on normalized Larmor radius was studied. The shots 23555 and 23556 are a pair with a low-triangularity (low-δ) configuration (Figure 3a). The shots 26177 and 26276 (27377 and 27390) are a pair with a high-δ configuration (Figure 3b). Deuterium neutral beams with parallel (//) and perpendicular (⊥) injection angles were injected into a deuterium plasma. Beam lines are shown in the figure. Pedestal data for shots 23555, 23556, 27377 and 27390 have been supplied. Profiles of electron density and electron temperature were obtained by Thomson scattering measurement. The electron cyclotron emission (ECE) measurement was also used for T_e profile. The ion temperature was measured by charge-exchange-recombination spectroscopy (CXRS).

A further 46 data entries from 16 H-Mode physics discharges (shots #33635-33670) were supplied from JT-60U experiments in 1999 [50,51]. The experiments were carried out at I = 1.8 MA, B = 3.0 T and q_{95} = 2.9-3.1. The wall condition was kept constant throughout this series of experiments. The divertor configuration had been modified from an open one to a W-shaped one. The plasma configuration and viewing chords of the main diagnostics are shown in Figure 2. The neutral beam injection power was varied in steps during a discharge from 4 to 13 MW. The line average electron density was varied on a shot by shot basis from 2.4_10^{19} to 4.5_10^{19}.m^{-3} ($n = 0.5 \cdot n_{GDL}$). Density was increased by deuterium gas puffing at the beginning of a discharge, and was kept almost constant during t = 6.0-8.5 s with the beam fuelling. Pedestal data for all the 1999 entries was also supplied.

2.7 MAST

Quasi-stationary H-mode plasmas have been produced on MAST in order to satisfy the conditions for the ITPA database. In particular the aim is to establish plasmas that are quasi-

stationary for the maximum possible period to reduce the uncertainties due to the time derivatives.

The data represent quasi-stationary ELMy plasmas, however, the ELMs are irregular. The increase of ELM frequency with increasing power, a typical characteristic of type I ELMs, has not yet been observed. The dataset consists of plasmas with and without sawteeth. The shots with sawteeth can suffer from the presence of neoclassical tearing modes and thus recent operation concentrated on scenario without sawteeth or large MHD activity. The $\boldsymbol{q}$-profiles estimated from EFIT equilibrium reconstruction using magnetic signals are monotonic and no internal transport barriers are observed in this dataset. The time of data extraction is selected so that the rate of change of energy content is smaller than 15% of the power loss and is close to the measurement time of high spatial resolution Thomson scattering and charge exchange diagnostics. The dataset covers the engineering parameter range of $\boldsymbol{I} = 0.73 - 0.78$ MA, $\boldsymbol{R} = 0.8 - 0.83$ m, $\boldsymbol{a} = 0.54 - 0.57$ m, $\kappa = 1.9 - 2.0$, $\boldsymbol{B} = 0.45 - 0.49$ T, $\boldsymbol{n} = (3.0 - 5.4) \times 10^{19}$ .m^{-3} and $\boldsymbol{P} = 1.5 - 3.0$ MW. All data are with the double null divertor configuration. The working gas is deuterium and plasmas are heated with neutral beams with energy 40 keV. Typically one of the two beam lines is operated in hydrogen to improve the ion temperature measurement but nevertheless the neutral particle analyser shows that the effective mass is $\boldsymbol{M} = 1.94 - 2.0$. The effective charge measured by bremsstrahlung emission at mid radius is $Z_{eff} = 1.1 - 1.4$.

The thermal energy confinement time has been deduced as $\tau_E = W_{th} / P_{L,th}$, where $W_{th} = \boldsymbol{W_{MHD}} - \boldsymbol{W_{FAST}}$ and $P_{L,th} = P_{oh} + \boldsymbol{P_{NBI}} - dW_{MHD}/dt$. Here, W_{MHD} is the energy content determined from EFIT equilibrium reconstruction. Fast ion energy content W_F and absorbed beam power $\boldsymbol{P_{NBI}}$ are deduced from TRANSP analysis [52]. The contribution of rotation to the energy content is small ($\approx$ 7%). The power loss due to shine through, charge exchange and orbit loss is several percent in total. The beam heating power is approximately equally distributed between electrons and ions [53]. The total radiated power is below 15% and is not allowed for when calculating the confinement time, in line with the convention of the international database. The energy content W_{MHD} from magnetic reconstruction is that calculated by TRANSP using kinetic profiles agree within ± 10%.

It is found that the fast ion content increases as plasma collisionality decreases. In order to limit the uncertainty in thermal energy confinement and also exclude the possible effect of fast particles on heat transport the selected data have been limited to $\boldsymbol{W_{FAST}} / \boldsymbol{W_{MHD}} < 35\%$. This

basically defines the lower limit on density range in the dataset as specified above. More details can be found in Ref. 54.

For the pedestal database, five shots have been selected from quasi stationary ELMy H-mode database. These are all double null plasmas, NBI heated (deuterium into deuterium), with $\boldsymbol{I} \approx$ 700 kA and $\boldsymbol{P_{NBI}} > 1.4$ MW. For a detailed description of these plasmas, see Ref. 55. The power through the boundary is calculated as:

$$\mathrm{PL} = \mathrm{POHM} + \mathrm{PINJ} - \mathrm{DWMHD} - \mathrm{PRAD}$$

How much power flows along the thermal channel remains to be determined, but kinetic analysis [55] suggests that the contribution of fast ions is not higher than ≈10% so the approximation $\mathrm{PLTH} = \mathrm{PL}$ may be taken.

The pedestal profiles are determined from a Thomson scattering system with high spatial resolution in a single shot. The pedestal position is determined by fitting the function $a \cdot \tanh\left[\left(\psi_N - \psi_0\right)/\Delta\right] + b$ (4 parameter-fit: $\boldsymbol{a}$, ψ_0, Δ, $\boldsymbol{b}$) to the inboard density profile from Thomson Scattering measurements mapped to the normalised poloidal flux ψ_N. The pedestal position is then calculated using the formula: $\psi_{N,ped} = \psi_0 - 2.5 \cdot \Delta$.

The EFIT reconstruction uses magnetics measurements together with 6 additional parameters. These are determined from the Thomson scattering temperature profile: position of magnetic axis, inboard and outboard separatrix positions and 3 pairs of points (inboard and outboard) having the same temperature (hence assumed to be lying on the same flux surface). Some of the entries use equilibriums calculated from a standard EFIT reconstruction with only magnetic measurements. A comparison shows that adding additional constraints to EFIT makes very small difference in calculated pedestal parameters for shots selected.

The fits are shown in Figure 1. These show electron density, temperature and pressure mapped to the poloidal flux. The Thomson scattering system measures the parameters radially in the midplane $\left(\boldsymbol{R}, \boldsymbol{Z} = 0\right)$. In addition to inboard values (circles) the outboard parameters are shown for comparison (squares). The spatial resolution of outboard points, however, needs more detailed analysis.

The values of $\psi_{N,ped}$ are supplied in a new variable PSIPED. Generally the above procedure locates the pedestal to $\psi_{N,ped} \approx 0.97$.

It should be noted that the MAST pedestal measurements supplied are not averaged over ELMs. However, the temporal location of a Thomson scattering measurement relative to an ELM is random and therefore the dataset is a good representation of averaged pedestal profile.

So far, no saturation in the TEPED-NEPED diagram has been observed on MAST. Also, no increase of ELM frequency with the heating power, a common signature of type I ELMs, has been seen on MAST.

2.8 NSTX

The low-aspect ratio NSTX contribution to the DB3V13 H-mode database consisted of seven time slices taken from seven discharges. The discharges were taken from operating periods during 2001-2002. All of the discharges were run in the Lower Single Null configuration, with the X-point in the direction of the ion grad-B drift. Six of the discharges had small, high frequency ELMs, while one was ELM-free. The NSTX vessel has a set of close-fitting copper passive stabilizer plates on the outboard plasma side, with graphite tiles protecting the copper from the plasma.

The data cover the ranges in global parameters: $\boldsymbol{R}$ = 0.87 m, $\boldsymbol{a}$ = 0.58 to 0.65 m (aspect ratio, $\boldsymbol{R/a}$, ≈ 1.33 to 1.5), $\boldsymbol{I}$ = 0.8 MA, $\boldsymbol{B}$ = 0.45 to 0.50 T, κ = 1.8 to 2.0, δ = 0.3, $\boldsymbol{n}$ = 4.5 to 6.5 _ 10^{19}.m^{-3} and $\boldsymbol{P}$ = 2.1 to 6.6 MW. All data have deuterium neutral beams injected into deuterium plasmas.

Experimental results showed that the plasma global confinement times were typically in excess of the twice the ITER97L L-mode scaling, reaching close to three times the scaling values, while the thermal confinement times reached 1.6 times the IPB98(y,2) scaling value.

The electron temperature and density profiles are measured on the midplane by a 20 radial point profile Thomson Scattering system with a time resolution of 16 ms. This diagnostic has recently been upgraded to a 30 radial point profile, with the additional 10 radial points being in the outer portion of the plasma for better diagnosis of the edge. Carbon temperature, toroidal rotation and impurity density profiles are measured by a 56 radial point Charge Exchange Recombination Spectroscopy diagnostic with time resolution down to 10 ms. The magnetic field pitch is measured by an 8-point Motional Stark Effect diagnostic. The radiated power is measured with an array of bolometers, and neutron emission by a collection of neutron monitors. Diamagnetic flux measurements are made, which are then input into equilibrium codes (EFIT,

LRDFIT) for time-dependent, between shots equilibrium reconstructions. MHD instabilities with frequencies up to several MHz are diagnosed by toroidal and poloidal arrays of Mirnov coils, and density fluctuations in the plasma core and edge are measured from low to high-k using Far-infrared interferometry, correlation reflectometry, reciprocating Langmuir probes, gas puff imaging and tangential scattering diagnostics.

Pedestal heights in NSTX for electron density and temperature are determined by the Thomson Scattering diagnostic. The profiles are fit to a 'standard' modified hyperbolic tangent as discussed in Groebner, *et al.* [56], with an example shown in Maingi, *et al.* [57]. The spatial resolution of the Thomson scattering diagnostic was upgraded in 2005 to approximately 1-1.5 cm near the edge, which enables measurement of the widths and gradients as well. In addition, the top of the ion temperature pedestal can be obtained in some cases by the CHERS diagnostic. In these cases, the top of the pedestal is identified by a substantial change in the ion temperature radial gradient.

2.9 START

The Small Tight Aspect Ratio Tokamak START was operational until 1998. Distinct features of these plasmas are the small aspect ratio (major and minor radii typically 0.30 and 0.21 m) and high values of toroidal beta (world record values of $\beta \approx 40\%$ being achieved [58]). Data from START, its successor MAST, and NSTX are extending the International database by a factor of two along the aspect ratio co-ordinate.

START data selected for the International database are a subset of a larger database of H-mode START data [59]. The selection procedure concentrated on a quasi-stationary ELMy H-mode regime with double null configuration. START plasma only occupied around 7% of the volume of the vacuum vessel and had an open divertor geometry. Regular boronisation was applied to the walls and helium glow discharge cleaning was used between the shots. The data represent ELMy H-modes with both Ohmic and neutral beam heating. A common feature of H-mode discharges in START was the presence of sawteeth. Although a sawtooth crash often triggered an ELM, the ELM frequency was considerably higher than that of the sawteeth.

Energy content was measured by magnetic reconstruction (EFIT). The density and temperature profiles were determined from a 30-point Thomson scattering system and from 20-chord charge exchange spectroscopy. The fast ion component was estimated self-consistently

and subtracted from the total plasma energy to determine the plasma thermal energy. The input power was taken as the sum of the Ohmic input and the NBI power absorbed, i.e. the shine-through and first orbit losses (which together could be as high as 50% in START) were subtracted.

2.10 T-10

T-10 is a limiter tokamak with circular cross section, major radius R = 1.5 m, and aspect ratio ≈ 5. The powerful ECR system is used for plasma auxiliary heating (ECRH) and current drive.

The contribution to H-mode database consists of four discharges with a transition to improved confinement regime. These discharges were obtained with ECRH in 1999 [60,61]. A characteristic feature of these shots is a spontaneous density growth accompanied by a drop in the intensity of D_α line and an increase in β by a factor of up to 1.7 in comparison with the pre-transition regime. Therefore these features are similar to that for H-mode. The additional feature of the T-10 H-mode is the existence of the hot spot on the high field side of the circular limiter [62]. The threshold power for the transition is close to that predicted by the ITER scaling for the L-H transition [63]. In the T-10 H-mode regime the external transport barrier acts on particles whereas the heat transport barrier only slightly contributes to the improved confinement.

The discharges represent a plasma current scan from 227 kA to 330 kA. The respective safety factor $q_{\lim iter}$ variations are from 3.2 to 2.2. The confinement improvement was more pronounced at the lower $q_{\lim iter}$ values. Three time slices are provided for each discharge: the Ohmic data before the ECRH start, L-mode data just before the L-H transition and H-mode data, which correspond to the end of the ECRH pulse. The experiments were carried out using a circular graphite poloidal limiter with radius 0.33 m and a bottom graphite mushroom-like limiter at $a_{\lim iter}$ = 0.3 m. The discharges are characterized by the same initial (L-mode) plasma density $n \cong 1.4\times10^{19}.\mathrm{m}^{-3}$, toroidal magnetic field B = 2.42 T, that corresponds to the on-axis ECRH and absorbed ECR power P_{ECRH} = 0.75 MW.

Plasma stored energy is determined from diamagnetic measurements. The density profiles are measured using 8 radially separated channels of a microwave interferometer with 2 additional channels of a HCN-interferometer located at the plasma outer third. Electron temperature profiles are measured by an 8 channel ECE diagnostic, located at the low field side of the plasma column. The thermal heat power is the sum of the Ohmic input and the ECRH power absorbed in

the plasma. The absorbed ECR power is calculated using the TORAY code [64]. The T-10 data were prepared using the transport code ASTRA [65].

2.11 TCV

TCV is a medium size tokamak with high plasma shaping capability and a powerful ECH system. TCV major and minor radii are $\boldsymbol{R}$ = 0.88 m and $\boldsymbol{a}$ = 0.25 m, respectively. 16 independent shaping coils located along a highly elongated vacuum vessel allow the creation of limited or diverted plasmas with KAPPA in the range 0.9-2.8 and DELTA in the range -0.4-0.9. The main magnetic field, $\boldsymbol{B}$, is generally set to 1.43 T and the plasma current, $\boldsymbol{I}$, is operated between 100 and 1000 kA. The electron line average density, NEL, ranges between 1 and 15 _ $10^{19}.m^{-3}$. The vacuum chamber has a rectangular cross section, its walls, floor and ceiling are almost totally covered by C-tiles and it is regularly conditioned by boronisations. There is no closed divertor, leaving the geometry of diverted plasmas very flexible.

The additional heating system resides in an ECH system comprised of 9 gyrotrons divided in two groups. A group of 6 gyrotrons is operated at the 2nd harmonic (82.7 GHz). Their beams are directed into the tokamak through lateral ports and the launcher system allows beam injection with variable poloidal and toroidal angles. This flexibility in the launching angles allows precise radial deposition and generation of toroidal current for current drive experiments. Another group of 3 gyrotrons is operated at the 3rd harmonic (118GHz). These beams are injected from the top of the vessel. A movable and tiltable mirror allows precise injection along the resonance layer. The 9 gyrotrons deliver up to 500 kW each, representing a total of up to 4.5 MW.

The diagnostics used to provide data to this database are: magnetic probes and flux loops for plasma current, position and shape; Thomson scattering system for electron temperature; FIR interferometer and/or Thomson scattering system for line average density and local density; magnetic measurements and Thomson scattering system for plasma energy, Ohmic power, confinement time and related variables; D-alpha signal for ELM variables.

Contributions to this version of the database are from purely Ohmic time slices, taken during ELM free or ELMy phases. The time slices are chosen in single null diverted discharges in the most steady state conditions.

2.12 TdeV

In TdeV, well controlled stationary H-modes exhibiting type III ELMs were obtained using ECRH (110 GHz, >150 kW) and LH (3.7 GHz, >300 kW). TdeV was a divertor configuration tokamak with $\boldsymbol{R}$ = 0.83 m, a = 0.21 m, $\boldsymbol{I}$ = 0.22 MA and $\boldsymbol{B}$ = 1.96 T operating in a single null configuration. The divertor was located at the top of the machine with an X-point slightly inside the major radius of the machine. Experiments were run at two plasma currents (160 and 220 kA), with the $\boldsymbol{B}\times\nabla\boldsymbol{B}$ drift both towards and away from the X-point and for two positions (by varying the mirror angle) of EC power deposition (vertically at 5 and 10 cm from the plasma centre).

Two methods were used to achieve H-modes in addition to auxiliary heating: varying the plasma lower triangularity and applying a positive biasing between the divertor plates and the vacuum chamber. Although it has been reported that H-modes do not require special wall conditioning (except for in the supershot regime) [66], a few helium discharge-cleaning plasmas were necessary before an H-mode was obtained and degradation could be seen in the quality of the H-modes between the beginning and the end of the day. The machine walls were boronised, reducing the oxygen and carbon impurities.

Typical features of the H-modes observed in TdeV were: a drop in the D_α radiation in the presence of ELM activity, a rise in the total stored energy and energy confinement time and a rise in the line average electron density (see Figure 4). The electron density and temperature profiles for H-modes obtained by varying the triangularity and the divertor plate bias are shown in Figure 5a and Figure 5b. Unfortunately the spatial resolution for both the interferometer and Thomson scattering diagnostics was too low to clearly see the presence of a pedestal inside the separatrix. The electron density profile measured by the reflectometer around the separatrix was observed to be steeper in the H-mode than in the L-mode (see Figure 5c).

For TdeV, the normal direction of the plasma current (the plasma current and the toroidal magnetic field directions were always the same) refers to the clockwise direction looking downwards; under these conditions the $\boldsymbol{B}\times\nabla\boldsymbol{B}$ drift was away from the divertor. The $\boldsymbol{B}\times\nabla\boldsymbol{B}$ drift toward the divertor was more favourable for the H-mode, but not optimal for the LH current drive. With this configuration, steady state H-modes (during all of the ECRH phase) were obtained with ECRH power by varying the bottom plasma triangularity and by applying a positive bias to the divertor plates. A few discharges with H modes induced by negative biasing were also achieved. In the discharges with the $\boldsymbol{B}\times\nabla\boldsymbol{B}$ drift away from the divertor, steady state H-modes could be obtained with ECRH only and combined ECRH and LH power by varying the

plasma triangularity. Oscillations between H and L with very short H-modes (50–100 ms) were obtained with both positive and negative divertor plate biasing. The observations for the discharges with the $\boldsymbol{B} \times \nabla \boldsymbol{B}$ drift towards the divertor confirmed the previous reports on TdeV H-modes in which it was concluded that positive biasing is favourable to H-modes, whereas negative biasing is detrimental [67]. These observations were repeated with the $\boldsymbol{B} \times \nabla \boldsymbol{B}$ drift away from the divertor, i.e. reversing the toroidal field polarity did not reverse the biasing effect.

2.13 TFTR

TFTR was a limiter tokamak which operated from 1982-1997. During this time it became the first machine to operate with 50%-50% deuterium-tritium plasmas, producing a maximum of 10.7 MW of fusion energy. TFTR H-mode plasmas were usually, but not always, produced by ramping down the plasma current during the NBI heating. This produced plasmas with high values of β_p and l_i, large Shafranov shift and increased magnetic shear particularly at the plasma edge.

For TFTR shots < 45000, the plasma geometry, RGEO, AMIN, and BEILI2, values currently in the database were obtained from measured moments of the external poloidal field using analytic expressions; KAPPA = 1 was assumed. For shots > 45000, the analysis to determine RGEO, AMIN, KAPPA and BEILI2, used a numerical mapping from the measured moments which was established by simulating the equilibrium for the TFTR coil set and limiters with a filament code for a range of values of BEILI2 and RGEO. The values for the early shots (< 45000) have now been recalculated, using the filament code as for the later shots, and the revised values for RGEO, AMIN, KAPPA, AREA and VOL are shown in Table 1. The other MHD quantities did not change by more than their quoted errors, which are given in Table 2.

The magnetic axis RMAG was calculated from RGEO, AMIN and BEILI2 with a model validated against experimental profiles and equilibrium calculations in the TRANSP code. The diamagnetic poloidal beta BEPDIA was determined from the displaced toroidal flux, measured with an accuracy of ± 1 mWb which in the H-mode discharges corresponds to an uncertainty of about 100 kJ in the "diamagnetic plasma energy", WDIA = 4.71 _ 10^{-7}.RGEO.IP^2.BEPDIA with the normalisation adopted for all TFTR data. The total plasma energy WTOT = 3.14 _ 10^{-7}.RGEO.IP^2.(BEPMHD + BEPDIA/2) where BEPMHD = BEILI2 - LI/2 was obtained using a model for the time evolution of the internal inductance LI during the NBI pulse. The LI model takes as boundary conditions the values obtained from the equation LI/2 = BEILI2 - BEPDIA

which is valid when the plasma pressure is isotropic before and after the NBI. In the H-mode current ramp-down shots, LI was interpolated with the variation of the edge q between the initial and final conditions [68]. This heuristic model was checked against calculations of LI in the TRANSP code based on solving the resistive diffusion equation for the toroidal current density based on neoclassical resistivity and the measured profiles. Although the current ramp-down employed to produce the H-mode was a challenging condition for the LI model, the values of LI/2 at the times in the H-mode database derived from the magnetic analysis agreed well with the TRANSP calculations; for the subset of 21 TFTR H-mode plasmas with full TRANSP analyses; the mean of the difference between the model and TRANSP LI/2 was 0.05 with a standard deviation of 0.1. This standard deviation was incorporated into the normal level of accuracy for the resultant parameters in the H-mode database.

The values of BEIMHD for the TFTR data appear to be (2.BEPMHD + BEPDIA)/3 so WTOT = 3.14 _ 10^{-7}.RGEO.IP^2.BEIMHD; this is not what is described in the variable definitions. All values of WMHD in the TFTR H-mode data are in fact WTOT values. The WMHD values should be corrected using WMHD = (3.WTOT – WDIA)/2 or equivalently WTOT.(BEPMHD/BEIMHD).

The cross section area in the database appears to be given by AREA = π.AMIN^2.KAPPA which is valid for TFTR. However, the volume in the database appears to be VOL = 2. π^2.RGEO.AMIN^2 which is missing the factor KAPPA. This should be corrected.

Note that the Ohmic power for TFTR data frequently appears negative, which is unphysical. This is due to the limitations of the calculation based on POHM = IP.VSURF – d(3.14 _ 10^{-7}.RGEO.IP^2.LI)/dt using the modelled LI(t). The POHM is generally small compared to the loss power, in the range –9% to +1%, mean –3%, standard deviation 1%, but it should be set to zero if negative.

2.14 TUMAN-3M

TUMAN-3M is a circular cross section tokamak without divertor [69]. The device has the following parameters: vessel major radius, R = 0.55 m, circular limiter radius, $a_{\lim iter}$ = 0.24 m, longitudinal magnetic field, $B \leq$ 1.2 T, plasma current, $I \leq$ 175 kA, line average density $n \leq$ 6.2 _ 10^{19}.m^{-3}, central electron temperature, $T_e(\psi = 0) \leq$ 1.0 keV, central ion temperature,

$T_i(\psi = 0) \leq 0.4$ keV. The vessel and circular limiters are made of Inconel (80% – Ni, 20% – Cr). The sector limiter (30° at the low field side, limiter shadow – 50 mm) is made of molybdenum.

Standard vessel conditioning consists of 3-4 hour AC inductive discharge cleaning with low toroidal current, $I_{cl} \cong 1$ kA, and low plasma temperature, $\langle T_e \rangle = 3$ - 10 eV in deuterium, followed by 2 - 3 hours baking with wall temperature ≤ 200°C. The procedure is used for everyday vessel preparation. From time to time (once in 300 - 2000 shots) boronisation is performed. The boronisation includes ≈ 1 hour of glow in He with admixture of Carborane ($C_2B_{10}H_{12}$) [70]. Typical Z_{eff} values in the TUMAN-3M plasma are below 2.0. In the freshly boronised vessel (first 300 - 500 shots) Z_{eff} is close to 1.0.

TUMAN-3M is equipped with the following diagnostic tools: magnetics (poloidal flux loops and coils, diamagnetic coils, 2 toroidally separated sets of 24 Mirnov coils, Rogowski coils), microwave interferometry (10 vertical equidistant channels with $\Delta R = 48$ mm, $\lambda_{RF} = 2.2$ mm), SXR diode array ($\Delta R = 30$ mm at equatorial plane), Thomson scattering (2×4 spatial channels, 5 spectrum channels, single pulse Ruby laser), neutral particle analyzer (2×6 energy channels, mass resolution), microwave reflectometry (RF frequency ≤ 26 GHz), D-alpha monitors. Other diagnostic tools are used occasionally (bolometry, heavy ion beam probe, Doppler shift visible spectroscopy, electrostatic probes).

Submissions to DB3 were taken from ELM-free Ohmic H-mode discharges [71]. In some shots the Ohmic H-mode developed spontaneously, but in the majority of the discharges the H-mode was induced by some increase in the working gas puffing rate (deuterium). The Ohmic H-mode was obtained at I =90-170 kA and $q_{cyl} = 2.1$-4.3, where $q_{cyl} = 5\kappa_a a^2 B/RI$ is equivalent to the safety factor for nested cylindrical surfaces. Submitted data include time slices (one slice per shot) in the shots with $I = 140$ - 165 kA, $q_{cyl} = 2.2$ - 2.9, $n = 0.8$ - 2.7 _ 10^{19}.m^{-3}. For some shots equilibrium simulations were performed in order to determine plasma geometry parameters. Energy content was measured with diamagnetic loops and was compared with kinetic measurements and equilibrium simulations in some shots. The data agree within 15% accuracy. Transition to the Ohmic H-mode results in a strong suppression of particle transport and a corresponding increase in the density. Reflectometry and probe measurements have shown significant drops in the peripheral turbulence after the H-mode transition.

3 THE NEW H-MODE DATABASE DB3V13

The final version of DB3, DB3v13, contains 10382 entries from 3717 discharges, which include Ohmic, L-mode, and H-mode experiments. This is approximately double the number of entries in DB2 [2]. ELMy H-modes, the focus of the confinement scaling work, account for 3813 entries from 2070 discharges. As the data contained in the full database are fairly broad, analyses usually begin with the imposition of several selection criteria to produce a reduced dataset suited to the problem of interest. The most common ones are given in the following section.

3.1 ELMy H-mode dataset selection criteria and weighting

The principal aim of the selections is to restrict variation in parameter ranges or modes of operation which may have different confinement properties to the bulk of the database. Thus, selection criteria reduce the hidden variables, which may affect energy confinement but are not included in the scalings.

3.1.1 The standard DB3 dataset

The selection criteria most commonly applied to DB3, and which will be referred to in this paper as the standard selection criteria, was first defined in Ref. 72 and when applied to the full DB3 produce a dataset [73,74] which will be referred to as the standard DB3 dataset. The selection criteria are a refinement of those used in earlier papers [1,2,66,72, 73,74,75,76,77,78,79] and can be summarised as:

i. ELMy H-mode discharges only without pellet fuelling and with all variables for confinement analysis present in the database. This includes type I, type III and EDA ELMy H-modes.

ii. Steady energy content: $-0.05 \le \frac{dW'}{dt} \Big/ P \le 0.35$. W' is defined as W_{MHD} or W_{DIA}, dependent on the machine. For TFTR this is relaxed to $-0.10 \le \frac{dW_{MHD}}{dt} \Big/ P \le 0.35$..

iii. Total radiated power less than 60% of injected power.

iv. $q_{95} \geq q_{crit}$, where q_{crit} is dependent on the machine. This results from the observed poor performance of plasmas, due to MHD activity, below a critical q-value.

v. Fast particles have less than 40% of the total plasma energy: $\boldsymbol{W_{FAST}} < 0.4 \cdot \boldsymbol{W}'$. $\boldsymbol{W}'$is defined as W_{MHD} or W_{DIA}, dependent on the machine. For TFTR this constraint is ignored.

vi. Plasma is well below the β limit. For PDX, $\beta_N < 4$, and for PBXM, $\beta_N < 2.8$. The other machines deselect shots near the β limit before submission.

vii. Core ion and electron temperatures do not vary by more that a factor of 2.5, i.e. $0.4 \leq T_i(\psi = 0)/T_e(\psi = 0) \leq 2.5$, and no Hot ion H-modes.

viii. Internal inductance limited by $l_i \leq 2$.

Exact details of these criteria, and how they should be applied to the database, are given in Appendix A. The standard dataset has 3093 entries from 2138 discharges. To ease the selection of the standard dataset, the variable IAE2004S has been included and selecting all DB3 shots where IAE2004S = 1 results in the selection of this dataset.

3.1.2 The non-Ohmic deuterium DB3 dataset

DB3 has been found to be rather poorly conditioned with respect to isotope mass [74], with 2394 of the 3093 entries in the standard set having $1.833 < M < 2.167$, which leads to large uncertainties in the derived mass scaling. One method for treating this is to ignore the mass scaling altogether by imposing the $1.833 < M < 2.167$ selection criteria on the dataset, to create an essentially deuterium only dataset and drop the mass variable from any derived scalings. This will be described in more detail in section 3.3. In addition, concerns over the natural correlation between Ohmic heating power and parameters such as plasma current, have led to selection criteria that remove purely Ohmic heated plasmas from the dataset. The imposition of both the isotope mass and non-Ohmic constraints, discussed above, on the standard dataset result in the non-Ohmic, deuterium dataset. The non-Ohmic, deuterium dataset has 2276 entries from 1727 discharges. To ease the selection of the non-Ohmic deuterium dataset, the variable DB3DONLY

has been included and selecting all DB3 shots where DB3DONLY = 1 results in the selection of this dataset.

3.1.3 The ITER-like DB3 dataset

To a lesser degree, the conditioning of the dataset with respect to elongation and safety factor has also been shown to be limited [74]. For the purposes of ITER scaling, one method used to disentangle the possible different scalings in near circular plasmas and elongated plasmas is to restrict the dataset to approximately ITER-like elongation and safety factor and drop these variables from the scalings. This has been done by taking the standard dataset with the additional three criteria.

a) $1.4 < \kappa < 1.93$,

b) $1.6 < q_{cyl} < 2.8$,

c) $1.833 < M < 2.167$.

The resulting dataset is known as the ITER-like dataset, which can be used to scale to deuterium only plasmas in ITER. The ITER-like dataset has 1458 entries from 1147 discharges. To ease the selection of the ITER-like dataset, the variable IAE2004I has been included and selecting all DB3 shots where IAE2004I = 1 results in the selection of this dataset.

3.1.4 Pedestal-global confinement DB3-PED DB3v2 dataset

The pedestal database is an independent database to the global confinement database, which contains parameters describing the pedestal properties of ELMy H-modes. The general analysis of this database [3,80,81] lies outside the scope of this paper, but its application to two-term scalings is considered here. For this work, the compilation of the two databases has been coordinated so that a significant fraction of entries are common to both. The common entries can then be combined to produce the pedestal-global confinement dataset. The latest version of the

pedestal database is PED DB3v2 whose intersection with DB3 results in a pedestal-global confinement dataset of 472 entries from 304 discharges. This represents data from the seven machines ASDEX Upgrade (114), C-Mod (19), DIII-D (90), JET (161), JFT-2M (1), JT-60U (82), and MAST (5).

3.2 Errors in parameters

An understanding of the errors on the database parameters is important both to establish the significance of correlations in the database and to estimate the errors in resulting scaling laws and extrapolations. For this reason, the fractional errors in the physics parameters commonly used in global confinement scalings derived from DB3 have been calculated individually for each machine [73,74]. These have then been combined to give estimates of the fractional errors for the whole database. The calculated values are summarised in Table 4. It can be seen that the variables with the largest errors are the loss power (14.2%) and the thermal energy (14.1%), with the rest being below 10%. However, it should be noted that, as a proper study of the sources of error within the individual machines would be extremely time consuming, the derived numbers are approximate estimates. In addition, the combining of the error estimates into a single fractional error for each variable is approximate at best. The values of these errors should thus be taken as first approximations.

3.3 Data range and condition of the datasets

The data range, in the standard dataset, of the main parameters used for confinement scalings is given in Table 3. Comparing with Table II of Ref. 2, it can be seen that, with the exception of plasma current, the range in all these parameters has been extended. In particular, with the inclusion of JET tritium discharges, the range in isotope mass, $\boldsymbol{M}$, has increased from 1.0-2.0 to 1.0-3.0. With the inclusion of C-Mod, COMPASS, MAST, NSTX, START, TCV, TdeV, diverted JET and JT-60U and data, the range in R has increased from 1.29-2.93 to 0.28-3.4. With the inclusion of COMPASS and START data, the energy confinement time, τ_E, has increased from 0.012-1.32 s to 0.0022-1.32 s, and now covers almost three orders of magnitude. The range in inverse aspect ratio, ε, has increased from 0.16-0.41 to 0.16-0.78, with the

inclusion of START, MAST and NSTX data. Qualitatively speaking, these increases in the data range lead to greater confidence in the scalings derived from the database, notably for mass, aspect ratio and, most importantly for extrapolation to ITER, size.

To study the suitability of the database for empirical scalings in a more systematic way, the standard approach has been to use a Principal Components Analysis [1,82,73,74] (PCA). Crudely, this method takes the multi-dimensional parameters space of the logarithm of the variables to be used in a fit and finds the direction in which they have the greatest standard deviation (STD), which is then referred to as Principal Component 1 (PC1). The direction with greatest STD in a direction tangential to PC1 is then found and referred to as PC2. The process is then repeated, with each new Principal Component (PC) lying in the direction of the greatest STD in the data that is perpendicular to all the previous ones. The smallest PC represents the direction in which the data have the smallest STD.

The result of a PCA for the standard dataset is shown in Table 5. λ_{pc} denotes the STD of a PC, ignoring the effects of errors in the parameters, and λ_e denotes the STD in a given logged parameter, taken for DB3 from Table 4. An estimate of the STD of a PC including errors in the parameters can be shown to be $\lambda_e + \lambda_{pc}$ and the parameter $ERR = \lambda_e / (\lambda_e + \lambda_{pc})$ can be shown to be a measure of the bias on a standard Ordinary Least Squares (OLS) fit associated with a particular PC, with $ERR < 0.2$ indicating a bias of less than 6% [74,82]. It can be seen that all PCs have $ERR < 0.6$, but that two of the PCs, PC6 and PC8, have $ERR > 0.5$ and a total of five PCs have $ERR > 0.2$. This indicates that the dataset is only marginally suitable for fitting τ_E with the eight variables listed. The large contribution from isotopic mass in PC6 associates it with the small STD in $\boldsymbol{M}$ resulting from the large amount of deuterium only data in the dataset. The large contributions from the plasma cross-sectional area, A, and a in PC8 are believed to be associated with the relatively small STD in elongation. The low STD in safety factor contributes to the relatively high ERR for PC7.

Table 6 shows the results of the PCA for the non-Ohmic, deuterium only dataset. It can be seen that the number of PCs with $ERR > 0.2$ has reduced to four, indicating a slight improvement, but that there remain two PCs (PC6 and PC7) with $ERR > 0.5$. Again, the two largest PCs are associated with the small STDs in safety factor and elongation.

The results of the PCA for the ITER-like dataset are given in Table 7. It can be seen that this dataset is much better conditioned than either the standard dataset or the non-Ohmic, deuterium

dataset, with all of the PCs having $ERR < 0.26$. This implies that this dataset is reasonably well conditioned for five parameter fits involving I, n, P, R, and a.

For the pedestal-global confinement dataset, the relatively low number of entries, 472, would suggest that it is more poorly conditioned than the other datasets for multivariate fits. For this reason, only four variables, I, n, P, R, are considered. Table 8 shows the results of a PCA for the pedestal-global confinement dataset with these four variables. It can be seen that one PC, PC3, already has $ERR = 0.37$ indicating that the dataset is marginal even for OLS fits involving only four variables.

4 POWER LAW SCALING OF THE ENERGY CONFINEMENT TIME

Determination of the energy confinement time, and its extrapolation to next step devices, is the principal aim of the ITPA Confinement Database Group. The most empirically direct way of doing is this is through a power law scaling of the form

$$\tau_E = \alpha_0 \cdot \prod_{j=1}^{J} X_j^{\alpha_j} , \qquad (2)$$

where X_j are the logged physical parameters in the fit, α_j are the exponential coefficients to be fitted, and J is the number of parameters in the fit. This form is both analytically convenient, as its logarithm reduces to a linear form, and well suited for extrapolation. The rest of this section will review the methods used for fitting power law scalings. Previous fits, performed on earlier versions of DB3, result in slightly different scalings to those from the full database, so the calculations and scalings will be repeated here for the definitive results.

At this point it should be noted that in all fits to the data, a correction is added to the confinement time of ASDEX discharges related to divertor type. Although, in general, divertor design has not been observed to have a strong effect on confinement, the ASDEX machine had an unusually large closed DIV-I divertor [83] leading to anomalously high confinement compared to that in other divertors. The expression $\tau_E^{ASDEX} = \tau_E / \left(C_{evap} \cdot C_{divertor} \right)$ is thus used, for

ASDEX data, with $C_{divertor} = 1.275$ for the closed (DV-I) ELMy ASDEX discharges; $C_{divertor} = 1.0$ for the others and $C_{evap} = 0.85(0.9)$ for the carbonised (boronised div-II) ASDEX discharges. The factor 1.275 has been taken from Ref. 11 with, from 2002 onward [84], a moderation of 0.85 accounting for the difference between `divertors in medium-sized and large machines' and the very open ASDEX divertor described in Ref. [85]. The estimated uncertainty (1 STD) in $TAUC92 = 1/(C_{evap} \cdot C_{divertor})$ is at present some 10%.

4.1 Ordinary Least Squares fits

OLS fitting of the logarithm of physics parameters to the H-mode Database is the standard method for performing such fits and has been used since the databases inception. As discussed above, the logarithm of power law scalings becomes a linear equation and, as a result, an OLS fit involves simply the inversion of a $J \times J$ matrix. Such OLS analyses have often been performed numerically with the SAS statistical software package [86].

The wide variety of the number of entries in DB3 for a given machine has led to concern that the machines with larger data entries may bias the fits. This has been resolved by using a weighting factor for each piece of data in the fits based on the number entries from the machine it belongs to. The weighting factors used are given by $w_i = 1/(2 + Int(\sqrt{N_i}/4))$, where, N_i are the number of data points in the database from a given machine, and $Int(x)$ denotes the nearest whole integer to the real number x. The weights used for the three global confinement datasets in this paper are given in Table 10.

The currently recommended scaling, IPB98(y,2),

$$\tau_{IPB98(y,2)} \equiv 5.62 \times 10^{-2} \cdot I^{0.93} B^{0.15} P^{-0.69} n^{0.41} M^{0.19} R^{1.97} \varepsilon^{0.58} \kappa_a^{0.78}, \quad (3)$$

was derived by an OLS fit to version 5 of DB3 using a similar selection criteria to the standard selection criteria [66]. Here, $\kappa_a = V/(2\pi^2 a^2 R)$ is an elongation measurement.

Performing weighted OLS fits for the three global confinement datasets discussed in Section 3.1 results in the following three scalings,

$$\tau_{OLS,Std} \equiv 5.93\times10^{-2}\cdot I^{0.86}B^{0.21}P^{-0.65}n^{0.39}M^{0.08}R^{1.99}\varepsilon^{0.68}\kappa_a{}^{0.84}, \quad (4a)$$

$$\tau_{OLS,D-only} \equiv 7.08\times10^{-2}\cdot I^{0.94}B^{0.13}P^{-0.65}n^{0.36}R^{1.81}\varepsilon^{0.55}\kappa_a{}^{0.76}, \quad (4b)$$

$$\tau_{OLS,ITER-like} \equiv 9.57\times10^{-2}\cdot I^{1.06}P^{-0.61}n^{0.39}R^{1.78}\varepsilon^{0.56}. \quad (4c)$$

It can be seen that the largest variation in the fitted exponents, between the fits to the three datasets and IPB98(y,2), is 0.22 for the R scaling, indicating a certain robustness of the fits to the data used. A direct comparison of the scalings with the data, Figure 6, Figure 7 and Figure 8, also indicates that they have similar agreement, with similar Root Mean Squared Errors (RMSE) of 17.4%, for Equation 4a, 17.5%, for Equation 4b, and 18.0%, for Equation 4c. However, the scalings do clearly differ to some degree, indicating some sensitivity to the dataset used and/or the precise form of the variables chosen for the fit.

4.2 Errors in Variables fits

One concern with OLS fits is that they are known to give biased results when the measurement errors in the variables being fitted become comparable to those for the variable which is being fitted to [87]. For the fits of Section 4.1, this means that the measurement error in $\boldsymbol{W}$ must be considerably larger than the errors for the other variables in the fit. Table 4 shows that this is not generally satisfied, as the estimated measurement error in $\boldsymbol{W}$, 14.1%, is comparable in size to that for P, 14.2%. To assess the impact of this bias, fits have been performed [73,74] using an Errors in Variables (EIV) method [82] which includes the estimated errors on all the parameters in the fit self consistently. Performing such a fit for the standard dataset gives,

$$\tau_{EIV,Std} \equiv 5.55\times10^{-2}\cdot I^{0.75}B^{0.32}P^{-0.62}n^{0.35}M^{0.06}R^{2.00}\varepsilon^{0.76}\kappa_a{}^{1.14}. \quad (5)$$

It can be seen that most of the coefficients in this fit are in line with the OLS fit of Equation 4a, with the exception of the I, B, and κ_a coefficients, which reflects the poor condition of this

dataset with respect to safety factor and elongation. The scaling of Equation 5 agrees well, however, with that of Equation 4c, derived from the ITER-like dataset, where it must be noted that the exponents of I and B in Equation 5 must be summed for comparison with a scaling at fixed safety factor. The RMSE of the fit is 17.8%, slightly larger than the fit of Equation 4a, reflecting the fact that, as errors on all the parameters are now being considered, the RMSE on τ_E is no longer a good statistic of the goodness of the fit.

Although EIV fits are more sophisticated that OLS fits, a good knowledge of the underlying measurement errors is required before they can be used to extrapolate with any confidence. It has already been seen, in Section 3.2, that the errors used for DB3 are approximate estimates, so this is clearly a cause for concern. As a test of the sensitivity to the measurement error estimates, the effect of varying the measurement errors on the EIV fits has been studied [73,74]. Figure 10 shows the result of varying the errors in both δW and δP whilst leaving the other variables fixed to their values in Table 4. The scalings in P, R and n are all seen to vary at the ± 0.1 level as the errors in both δW and δP are varied by 50%. In the limit where δW becomes large, it can be seen that the coefficients tend to their OLS values, given in Equation 4a.

EIV analyses demonstrate that the measurement errors in the fitted parameters do indeed lead to biasing in the OLS fits, typically at the level of ± 0.1 in their exponents. However, until a more reliable method of assessing the measurement errors has been established, it is not clear that a given EIV scaling should be used in preference to an OLS scaling.

As well as OLS and EIV, Bayesian methods [88,89] have also been applied to confinement scalings, for a database comprised of data taken from stellarators [90]. Some preliminary Bayesian analysis of the H-mode Database has also been performed [91], and this work is expected to continue in the coming years.

4.3 Dimensionless parameters

If energy confinement is assumed to be dominated by fully ionised, quasi-neutral plasma physics, then it can be shown [37] that a constraint, known as the Kadomtsev constraint, can be placed on derived scalings which removes one degree of freedom. Dedicated multi-machine dimensionless parameter identity experiments [92,93,94,44] have shown that this constraint is indeed satisfied for ELMy H-mode plasma confinement. Empirical fits to DB2 tended not to

satisfy the Kadomtsev constraint but, probably because of its better conditioning, fits to DB3 do [66]. One important consequence of the Kadomtsev constraint is that confinement scalings may be expressed in terms of non-dimensional parameters:

$$\omega_{ci} \cdot \tau_E = F(\rho^*, \beta, \nu^*; q, \varepsilon, \kappa, M, ...), \qquad (6)$$

where ω_{ci} is the ion Larmor gyro-frequency, $\rho^* = \rho_{Ti}/a$ is the normalised ion Larmor radius, $\beta = 2\mu_0 \boldsymbol{p}/\boldsymbol{B}^2$ is the normalised plasma pressure, $\nu^* = (\nu_{ei}/\varepsilon)/\omega_{Tbi}$ is the normalised collision frequency, ρ_{Ti} is the thermal ion Larmor radius, μ_0 is the permeability of the vacuum, p is the plasma thermal pressure, ν_{ei} is the ion-electron collision rate, and ω_{Tbi} is the thermal ion bounce frequency. There is some freedom in the choice of the dimensionless parameters, but the standard set taken here have been shown to be convenient for separating classes of physics models [38].

IPB98(y,2) expressed in dimensionless parameters is

$$\omega_{ci} \cdot \tau_{IPB98(y,2)} \propto \rho^{*-2.70} \beta^{-0.90} \nu^{*-0.01} M^{0.96} q^{-3.0} \varepsilon^{0.73} \kappa_a^{3.3}, \quad (7)$$

where it should be noted that the exponent on the elongation scaling was reported incorrectly as 2.3 in Ref. 66. In common with all scalings derived from DB3, the ρ^* scaling is close to $\omega_{ci} \cdot \tau_E \propto \rho^{*-3}$, a gyro-Bohm like scaling [95]. The almost negligible negative ν^* dependence of confinement seen in IPB98(y,2) contrasts with the stronger negative dependence seen in dedicated experiments on other machines [40,17,49,10,96] , although the observed scalings vary between the machines themselves. More problematical is the negative dependence of energy confinement on β which has been the subject of much investigation [94,41,97,16,98,51,99].

A strong degradation of energy confinement with β can be taken as evidence for dominant electromagnetic transport, whereas β independence is more consistent with electrostatic transport models [16]. At fixed field and size, the fusion product may be written as

$n \cdot T \cdot \tau_E \propto \beta \cdot \tau_E$, implying that high β operation of burning plasmas is strongly advantageous if energy confinement is β independent, but less so if energy confinement falls with increasing β. For these two reasons, the scaling of energy confinement with β has taken on a considerable importance. As with IPB98(y,2), OLS fits to DB3 all show an exponent on the β term which approaches -1. However, two series of dedicated experiments on both JET and DIII-D [94,16,98,41] have all shown a negligible dependence of normalised energy confinement on β. EIV analyses of DB3 have been shown to have weaker dependences on β [74] with, for example, the fit of Equation 5 resulting in a non-dimensional form of

$$\omega_{ci} \cdot \tau_{EIV,Std} \propto \rho^{*-2.78} \beta^{-0.20} \nu^{*-0.20}. \qquad (8)$$

If the assumed error on P is increased even further, the β dependence is removed altogether. More recently, however, experiments on JT-60U [51] have shown a negative dependence of energy confinement on β: going as $\omega_{ci} \cdot \tau_E \propto \beta^{-0.6}$. An analysis of DB3 entries for ASDEX Upgrade, JET and JT-60 U has indicated that this may be related to a change in the β dependence with triangularity, but further experiments are required to test this theory. A further complication to this issue is that the strong correlation between β and ε [94] resulting from the largest β values being reached on the tight aspect ratio machines START, MAST, and NSTX. This has been shown to make the determination of the exponents on β and ε difficult to obtain from fits to DB3 [100,91].

The scaling of energy confinement derived from OLS fits to IPB98(y,2) with M, q and κ have all been shown to be broadly consistent with dedicated scan experiments. A good review of these experiments is given in Ref. 101.

4.4 Alternative physical fitting parameters

The engineering parameters I, B, P, n, M, R, ε and κ_a are believed to be the main variables upon which energy confinement depends. This is born out, to some extent, by the

<20% scatter in the energy confinement time about that predicted from fits to these variables. However, several additional variables have also been investigated, driven by either theoretical or experimental considerations.

A decrease in energy confinement, relative to scaling laws, with increasing density has been observed for gas-fuelled density scans on several machines [26,102,99]. This has been attributed to a negative dependence of energy confinement on the neutral particle density at the plasma edge. Although well accepted, this result would appear to contradict the observation that energy confinement is dominated by fully ionised plasma physics. A study of DB3 supports a fall in confinement with increasing gas fuelling [99], but a suitable variable for describing the impact of fuelling has not yet been identified. At present, gas fuelled discharges are included in the standard sets, but some scalings have attempted to avoid the impact of gas fuelling simply by excluding these discharges [72].

Triangularity is observed to affect plasma confinement [103,26,104,102,24] and studies of DB3 are consistent with this. Studies on DB3 have shown only a very weak, often negligible, dependence of energy confinement on triangularity. Thus, triangularity has not been incorporated into the recommended scalings.

The ratio of ion to electron temperature has also been widely studied experimentally [105,106,107] and in all cases energy confinement is found to increase with increasing T_i/T_e . This effect has not been included in the fits, largely because of the lack of ion temperature data for most machines in DB3. However, discharges which are very different from $T_i = T_e$ are excluded from the standard dataset.

Plasma rotation has also been seen to be strongly correlated with energy confinement experimentally [108,109,110,111,112,113], but the lack of rotation data in DB3 means that this cannot, as yet, be studied with this database.

Studies of Helium-4 plasmas on JET have found that Helium-4 plasmas have energy confinement times below that of hydrogenic plasmas, $\tau_{E,He-4}/\tau_{IPB98(y,2)} = 0.77 \pm 0.04$ [30]. If energy confinement is assumed to be dominated by the physics of fully ionised plasmas, this can be interpreted as increasing isotopic charge, Z, having a negative impact on energy confinement. The JET Helium-4 data are included in the database, but a lack of data from other experiments means that a Z scaling has not been introduced. Alternatively, the difference

between Helium-4 and hydrogenic plasma confinement can be interpreted as being due atomic physics effects. It is not clear how to account for such effects in scaling laws.

Wall material, wall coating material and wall conditioning are also known to have an impact on energy confinement. Several machines find that boronisation and/or glow discharge cleaning are vital for achieving good quality H-modes – see Ref. 2 and Section 2. However, the processes by which the wall affects confinement are complicated and it is not clear which variable/variables should be chosen to represent them, so they do not naturally lend themselves to scaling analysis. Assuming that the wall impacts on the plasma confinement through impurities, Z-effective may be a suitable variable. Experimental studies in RTP indicate that the effect is fairly weak with $\tau_E \propto Z_{eff}^{0.09\pm0.03}$ for a scan in ECR heated L-modes [114]. Although Z-effective is included in DB3, it is not used in the scalings. No formal limit is placed on Z-effective in the selection criteria, but the condition that the radiated power remains below 60% of the total input power, does place a mild restriction on the impurity level in the standard DB3 dataset.

5 POWER LAW SCALINGS OF THE PEDESTAL ENERGY AND CORE-PEDESTAL MODELS OF ENERGY CONFINEMENT

Energy confinement in H-mode plasmas is determined by the transport properties of both the core and pedestal regions. This has been reflected in confinement scalings by the development of two-term models [115,78,79,3]. Two-term models divide the plasma into an outer pedestal region, with thermal energy W_{ped}, and a core region, with thermal energy W_{core}, that lies within it, Figure 11. The lack of a good estimate for the error on W_{ped} in the pedestal database means that Errors in Variables analyses can not yet be applied, so fits to W_{ped} are performed using OLS.

5.1 Fits to the full global-pedestal dataset

For pedestal scalings, both thermal conduction models and MHD limit models have been used to determine the pedestal energy, W_{ped}. Thermal conduction models assume that the pedestal energy is dominated by thermal transport and result in power law scalings that are similar in

form to those for global confinement derived in Section 4. MHD limit models assume that the pedestal gradient is limited by MHD activity and combine this with an expression for the pedestal width. The pedestal width is usually taken to be independent of power flux, which results in W_{ped} scalings that are independent of P. For PED DB3v2, the pedestal scaling that resulted in the two-term model with the lowest RMSE when fitted to DB3 was a thermal conduction model. This had the scaling,

$$\boldsymbol{W_{ped,1}} \equiv 6.43\times10^{-4}\cdot \boldsymbol{I}^{1.58}\boldsymbol{B}^{0.06}\boldsymbol{P}^{0.42}\boldsymbol{n}^{-0.08}\boldsymbol{M}^{0.2}\boldsymbol{R}^{1.08}\varepsilon^{-2.13}\kappa_a^{\,1.81}\boldsymbol{F_q}^{2.09}, \quad (9)$$

where $F_q = q_{95}/q_{cyl}$ is a shaping factor and $q_{cyl} = 5\kappa_a a^2 B/RI$ is equivalent to the safety factor for nested cylindrical surfaces. The RMSE of this fit is 23.5%. The fit is performed with 9 variables for which, with regard to the PCA of Section 3.3, the database is poorly conditioned – see Table 8. The resulting scaling is thus not well suited to extrapolation.

The scaling of the plasma core is derived from the wider global confinement dataset by a direct fit to $W_{core} = W - W_{ped}$. For the pedestal scaling of Equation 9, this results in

$$W_{core,1} \equiv 1.03\times10^{-1}\cdot I^{0.88}B^{0.11}P^{0.25}n^{0.49}M^{0.23}R^{2.02}\varepsilon^{1.22}\kappa_a^{\,0.24}, \quad (10)$$

This clearly differs from the global scaling of Equation 4a, suggesting a difference between core and global scalings. However, the form of the core scalings has been found to be very sensitive to the pedestal scaling used [78,79].

The derived pedestal and core scalings can now be combined into a two-term scaling. For the pedestal and core scalings of Equations 9 and 10 this results can be written as,

$$\boldsymbol{\tau_{two-term}} \equiv \frac{\boldsymbol{W_{ped,1}} + \boldsymbol{W_{core,1}}}{\boldsymbol{P}}, \quad (11)$$

The RMSE of this two-term scaling is 24.5%, in contrast to 16.6% for the OLS fit of Equation 4a. This increase in RMSE indicates that, although the two-term scaling contains a better physics representation of the ELMy H-mode confinement, it does not give a better fit to the experimental data.

The relation between the core and pedestal terms in the two-term scalings is linked to the phenomenon of profile stiffness [116], where energy transport increases dramatically above a critical temperature gradient, resulting in a fixed temperature profile. If the temperature profiles of all of the discharges in DB3 were perfectly stiff in the core region, the core scaling with power would be expected to be essentially the same as for the pedestal. Comparison of Equations 9 and 10 shows that the core and edge power scalings do differ to some extent. However, the poor condition of the pedestal database means that it is not possible to conclude that DB3 discharges are not perfectly stiff with any confidence. More detailed studies of the level of profile stiffness observed experimentally, indicate that there is no evidence of an inconsistency with confinement scalings [117].

5.2 Fits to an ITER-like dataset

As for the global database, the condition of the pedestal dataset can be improved by restricting the range of the data in a subset of the variables. This has been done by imposing the ITER-like constraints

a) $1.4 < \kappa < 1.85$,

b) $1.6 < q_{cyl} < 2.5$,

c) $1.833 < M < 2.167$.

on the pedestal-global confinement dataset. The resulting dataset will be referred to as the ITER-like pedestal-confinement dataset. This dataset contains 253 discharges, which can then be fitted with the five variables I, n, P, R and a. The results of PCA for the ITER-like pedestal-confinement dataset are given in Table 9. All the principal components in the ITER-like pedestal-confinement dataset have $ERR \leq 0.51$ in contrast to the full pedestal-confinement

dataset, Table 8, which has $ERR > 0.51$ for 6 of its 9 PCs. This indicates that the ITER-like pedestal-confinement dataset is considerably better conditioned than the full dataset. However, it should be noted that the ITER-like pedestal-confinement dataset still contains significant PCAs, 3 with $ERR > 0.3$, indicating that it is still far from perfectly conditioned.

Performing an OLS fit of the pedestal energy to I, n, P, R and a, for the ITER-like pedestal-confinement dataset, results in a scaling of

$$W_{ped,ITER-like} \equiv 2.40 \times 10^{-2} \cdot I^{1.64} P^{0.56} n^{-0.18} R^{1.03} \varepsilon^{-0.39} \qquad (12)$$

Although the I, n, P and R scalings remain close to those from the fit to the full pedestal-confinement dataset, Equation 9, the aspect ratio scaling has changed markedly. Subtracting $W_{ped,ITER-like}$ from the global thermal energy for the ITER-like global dataset and performing an EIV fit to I, n, P, R and a, using the errors given in Table 4, results in a scaling of

$$W_{core,ITER-like} \equiv 6.93 \times 10^{-2} \cdot I^{0.62} P^{0.47} n^{0.64} R^{2.12} \varepsilon^{1.15}. \qquad (13)$$

This differs from the scaling of Equation 10, particularly with respect to the power, current and density scalings. Again, the scalings for the core and pedestal can be combined to give a two-term scaling for the global confinement. The RMSE for this scaling, with respect to the global ITER-like dataset, is 18.4%, in contrast to 18.0% for the global scaling of Equation 4c. This indicates that there is little difference in the quality of fit of the two scalings. Although the two-term scaling has introduced more physics, it does not represent a better description of the global data.

When expressed in dimensionless variables, the confinement times for the pedestal and core regions become

$$\omega_{ci} \cdot \tau_{ped,ITER-like} \propto \rho^{*-2.89} \beta^{-0.52} \nu^{*-0.59}, \qquad (14a)$$

$$\omega_{ci} \cdot \tau_{core,ITER-like} \propto \rho^{*-2.82} \beta^{0.25} \nu^{*-0.02}. \qquad (14b)$$

The pedestal confinement is gyro-Bohm like, with negative dependencies on both β and ν^*. The core scaling is essentially gyro-Bohm like, with a weakly positive β dependence and negligible ν^* dependence.

It should be remembered that, as for the global ITER-like dataset, the two-term scaling derived from (12) and (13) is only appropriate for extrapolation to discharges that satisfy the constraints placed upon the dataset.

6 EXTRAPOLATION OF CONFINEMENT SCALINGS

The term "recommended" clearly denotes a subjective opinion. In the present context, it refers to the agreed opinion of the ITPA H-mode Database Working Group based on the analyses reviewed in this paper.

6.1 Recommended scalings

Studies of an early version (version 5) of DB3, resulted in the ITER Physics Basis 1998 ELMy H-mode scalings [66], commonly denoted IPB98(y). The IPB98(y) are a set of 5 scalings derived from OLS fits and separated by differing datasets and selection criteria. At the time of the original analysis, all five were seen as being of fairly equal merit. Subsequently, due to its better consistency with later versions of DB3, IPB98(y,2) has become the preferred scaling. IPB98(y,2) also describes the final version of DB3 well, with an RMSE of 17.48% which does not differ greatly from the RMSE of 17.42% seen for the OLS fit to the full DB3, Equation 4a. For this reason, IPB98(y,2) remains the recommended OLS scaling derived from the standard DB3 dataset.

However, as discussed in Section 4, OLS scalings derived from DB3 are likely to be biased due to the comparable size of the errors in the variables being fitted with the size of the error on the variable being fitted to. EIV scalings are better suited to such situations. As a result, the EIV scaling of Section 4.2, Equation 5, is seen as more reliable than the standard OLS fits. However,

while uncertainty exists in the size of the errors on the individual parameters themselves, it is not seen as reasonable to jettison IPB98(y,2).

The poor condition of the pedestal-global confinement dataset means that a fit to this dataset is not suitable for extrapolation. The ITER-like pedestal-global confinement dataset is significantly better conditioned and so the five variable fit to this, given in Section 5.2, is recommended, provided the extrapolation is restricted to plasmas that satisfy the additional constraints on this dataset. This, of course, is true by design for ITER. The poor condition of the pedestal-global confinement dataset means that the confidence placed in this scaling is less than that given to the global ones.

The recommended scalings are summarised below.

$$\tau_{IPB98(y,2)} \equiv 5.62\times10^{-2}\cdot I^{0.93}B^{0.15}P^{-0.69}n^{0.41}M^{0.19}R^{1.97}\varepsilon^{0.58}\kappa_a{}^{0.78}, \quad (15a)$$

$$\tau_{EIV,Std} \equiv 5.55\times10^{-2}\cdot I^{0.75}B^{0.32}P^{-0.62}n^{0.35}M^{0.06}R^{2.00}\varepsilon^{0.76}\kappa_a{}^{1.14}, \quad (15b)$$

$$\tau_{2term,ITER-like} \equiv 2.40\times10^{-2}\cdot I^{1.64}P^{-0.44}n^{-0.18}R^{1.03}\varepsilon^{-0.39} + 6.93\times10^{-2}\cdot I^{0.62}P^{-0.53}n^{0.64}R^{2.12}\varepsilon^{1.15}. \quad (15c)$$

These may be expressed in dimensionless parameters as,

$$\omega_{ci}\cdot\tau_{IPB98(y,2)} \propto \rho^{*-2.70}\,\beta^{-0.90}\nu^{*-0.01}, \quad (16a)$$

$$\omega_{ci}\cdot\tau_{EIV,Std} \propto \rho^{*-2.78}\,\beta^{-0.20}\nu^{*-0.20}, \quad (16b)$$

$$\omega_{ci}\cdot\tau_{ped,ITER-like} \propto \rho^{*-2.89}\,\beta^{-0.52}\nu^{*-0.59} + const\cdot\rho^{*-2.82}\,\beta^{0.25}\nu^{*-0.02}. \quad (16c)$$

Of these, the global scalings, 15a and 15b, are viewed with more confidence than the two-term scaling, 15c. Other scalings quoted in this paper are <u>not</u> recommended for extrapolations to future tokamak experiments.

6.2 Confidence intervals

For log-linear models it has been shown [1,75] that the confidence interval in predictions may be written as

$$\ln(\tau_E) \pm c \cdot \sum_{i=1}^{I} \sqrt{1 + \frac{\lambda_j^{\,2}}{\lambda_{pc,j}^{\,2}}} \,. \qquad (16)$$

Where $c = 4\sigma/\sqrt{N}$, σ is the RMSE of the fit, and N are the number of data points fitted. As described in detail in Ref. 1, the other variables in this equation relate to the J dimensional space of the logarithms of the fitted parameters, for which the PC vectors form an orthonormal basis. λ_j is then the distance of the measured point from the centre of this space along the j-th PC, and $\lambda_{pc,j}$ is the STD of the j-th PC.

A more sophisticated estimate of confidence intervals from scaling laws has considered log-nonlinear terms, the effect of removing individual machines from the dataset, and the effects of measurement errors [77]. In general, such considerations result in a widening of the error bars which increases as the extrapolation moves further from the dataset used.

6.3 Global scalings as constraints for 1D transport models

In the absence of a theoretically derived transport model that reliably predicts plasma confinement across a multi-machine database, analyses have been performed using 1D transport models that are constrained by global scalings. Such models explicitly give the same global confinement predictions as the global scalings on which they are based, but have the advantage that they also provide estimates of the associated thermal profiles. A variety of 1D transport models have been used in this context [118,119,120] ranging from simple analytical forms for the thermal diffusion coefficient to models derived from turbulent transport theory. In all cases, the calculated transport coefficients are then multiplied by a normalisation coefficient which

ensures that the global confinement, or core and pedestal confinement for two-term models, matches the global scaling. Such studies predict broadly similar fusion performance to that derived from the global scalings alone [121,119], indicating that the thermal profiles used for estimating fusion power production from global scalings is consistent with those derived from existing 1D models. However, such analyses are found to be sensitive to profile stiffness, with stiff transport models resulting in systematically higher temperature pedestals than those from non-stiff models. As for 0D modelling, this paper recommends the scalings of Section 6.1 for use as constraints for 1D transport models.

6.4 Impact on ITER

To determine the global performance of ITER, the confinement scaling must be solved self-consistently with a model which calculates the fusion power produced. Such studies, using the IPB98(y,2) scaling, have indicated that $Q = 10$ operation can be achieved in the ITER-like baseline scenario [66]. Analyses of this form lie outside the scope of this paper, but to assess the impact of the recommended scaling on ITER their predictions for one ITER relevant set of parameters can be compared. Table 12 quotes predicted confinement time from each of the recommended scalings, for the ITER-relevant parameters $\boldsymbol{I} = 15$ MA, $\boldsymbol{B} = 5.3$ T, $\boldsymbol{n} = 1.03 \times 10^{20} \cdot \mathrm{m}^{-3}$, $\boldsymbol{P} = 87$ MW, $\boldsymbol{R} = 6.2$ m, $\boldsymbol{a} = 2.0$ m, and $\kappa_a = 1.75$, which are associated with $Q = 10$ operation for the IPB98(y,2) scaling. For the global scalings, the prediction refers to a 50%-50% deuterium-tritium plasma, but for the two-term scaling, which only applies to deuterium plasmas, the result applies to a pure deuterium ITER discharge. As predicted mass scalings are weak, the differences are expected to be small. It can be seen that all three scalings give similar predictions, with τ_E in the range $3.29 - 3.90$ s. This indicates that all three scalings would predict $Q \approx 10$ operation for the baseline ITER scenario.

Fuller global performance analyses [98,74,42] have shown that the ITER operational space is sensitive to the β dependence of the confinement scaling, with fusion performance increasing with increasing β for scalings that are largely β independent, but not for confinement scalings that depend negatively on β. This suggests that the fits of Equations 15b and 15c, which both have a weaker β dependence than that of IPB98(y,2), would both predict improved performance at high β.

As indicated in Table 12, for IPB98(y,2), the estimated confinement time for the ITER baseline point is $\tau_{IPB98(y,2)} = 3.66$ s. Using the method described in Section 6.2, the associated 95% confidence interval has been estimated as $3.13 - 4.14$ s [122]. A similar analysis remains to be performed for the other scalings, but is expected to give a similar range.

1D transport studies of ITER, using models normalised to the IPB98(y,2) global scaling, have shown a range of fusion products from $Q = 4 - 5$ [119], for the Weiland [123] and GLF23 [124] models that exhibit profile stiffness, to $Q \geq 10$ for explicitly non-stiff models [118,121]. Normalisation to β independent global scalings [119] results in predictions of $Q \geq 10$, even for the Weiland and GLF23 models.

CONCLUSION

Data added since DB2, from ASDEX Upgrade, C-Mod, COMPASS-D, DIII-D, JET, JT-60U, MAST, NSTX, START, T-10, TCV, TdeV, TFTR, and TUMAN-3M, have been described. The resulting database, DB3, has been shown to have an increased range of data and, consequently, to have an improved condition. An Ordinary Least Squares fit to an early version of DB3 resulted in a scaling, IPB98(y,2), which has been shown to fit well with the standard dataset of the final version of DB3. Study of the errors in DB3 has led to the use of Errors in Variables methods, which are unbiased by the observed uncertainties in the fitted parameters. Analyses of these scalings, in terms of non-dimensional parameters, have been reviewed. Combining the database with the global pedestal database has resulted in two-term scalings which attempt to describe core and pedestal confinement separately, although the poor condition of this dataset means that such scalings are viewed as less reliable than the global ones. Techniques for extrapolating such scalings have been described. Compared to the IPB98(y,) scalings, the recommended scalings presented here give similar estimates for the energy confinement time of the ITER baseline scenario. The weaker β dependence of the scalings derived from DB3 indicates that confinement at high β_N is favourable for ITER, although uncertainty in the exact β scaling persists.

ACKNOWLEDGEMENTS

This work was partly funded jointly by the United Kingdom Engineering and Physical Sciences Research Council and by the European Communities under the contract of Association between EURATOM and UKAEA. The views and opinions expressed herein do not necessarily reflect those of the European Commission. This work was carried out within the framework of the European Fusion Development Agreement.

A. LIST OF VARIABLES FOR H-MODE CONFINEMENT DATABASE, DB3V13

The ITPA H-mode Confinement Database version 3, DB3, can be accessed from the website http://efdasql.ipp.mpg.de/HmodePublic/. The ITPA Pedestal Database version 3 can be accessed from the website http://efdasql.ipp.mpg.de/Peddb/. Both databases are available through an SQL server or in ASCII format. Additional information on the variables for each database is also given at these websites. It is strongly recommended that this paper is read before using this database.

DB3 comprises 164 variables, including the 111 variables in DB2 plus an additional 53 new variables. A further two variables have been renamed. The variables common to DB2 are described in Ref. 2. The new variables in DB3 are summarised in Table 13. 27 of the new variables reflect selection criteria, book keeping or H-factors, which are calculated directly from other variables. The remaining 26 reflect new physics. Of the selection criteria variables, 3 enable the datasets of this paper to be selected by placing the constraint that they be equal to 1. These are IAE2004S=1, for the standard DB3 dataset, DB3DONLY=1, for the non-Ohmic deuterium DB3 dataset, and IAE2004I=1, for the ITER-like DB3 dataset. Fuller details of the database variables, including a description of how they are derived for each machine, are given at the website.

SHOT	TIME	RGEO	AMIN	KAPPA	AREA	VOL
	[s]	[m]	[m]		[m^2]	[m^2]
42934	4.580	2.455	0.804	0.9237	1.887	29.08
44647	4.650	2.454	0.803	0.9597	1.957	30.12
44649	4.650	2.454	0.803	0.9624	1.960	30.17
44660	4.640	2.453	0.802	0.9579	1.948	29.98
44663	4.630	2.452	0.801	0.9578	1.944	29.90
44664	4.630	2.453	0.802	0.9554	1.944	29.92
44665	4.600	2.455	0.803	0.9602	1.959	30.16
44666	4.590	2.454	0.803	0.9604	1.956	30.11
44667	4.590	2.456	0.805	0.9702	1.987	30.60
44669	4.580	2.457	0.806	0.9684	1.988	30.64
44671	4.580	2.456	0.805	0.9679	1.982	30.53

Table 1: Recalculated geometric parameters for early TFTR H-mode shots

RGEO	1 cm
AMIN	1 cm
RMAG	4 cm
KAPPA	0.04
AREA	5%
VOL	6%
$\boldsymbol{B}$	2%
IP	2%
VSURF	0.05V + 5%
Q	6%
WDIA	100kJ + 4%
WTOT	100kJ + 6%
BEILI2	4%
BEPMHD	BEILI2*4% + 0.1
BEPDIA	100kJ/WDIA + 4%

Table 2: Normal level of accuracy for basic TFTR MHD data in H-mode database

Variable	Label	Mean	S. D.	Min.	Max.
BT	Toroidal field (T)	2.178	0.704	0.268	5.821
IP	Plasma current (MA)	1.418	0.935	0.159	5.134
NEL	Line average density ($10^{19}.m^{-3}$)	5.582	3.894	1.166	42.600
RGEO	Major radius (m)	2.232	0.709	0.280	3.400
AMIN	Minor radius (m)	0.685	0.254	0.159	1.133
KAPPA	Elongation	1.602	0.300	0.926	2.300
EPS	Inverse aspect ratio	0.305	0.058	0.155	0.783
Q95	q at the 95% flux surface	3.719	1.002	1.873	11.130
MEFF	1=H, 2=D, 3=T (average of plasma + beam)	1.882	0.280	1.000	2.988
PLTH	Total loss power	6.787	4.676	0.146	24.720
TAUTH	Thermal confinement time (s)	0.212	0.181	0.00224	1.321
WTH	Thermal energy (MJ)	1.859	2.035	0.00136	12.605

Table 3: Summary of key confinement parameters in the standard extended dataset of DB3.

Variable	δI	δB	δR	δn	δa	δM	δA	δW_{th}	δP
Error [%]	1.3	1.5	1.3	5.0	2.9	8.4	4.7	14.1	14.2

Table 4: Estimates of the measurement errors for the regression variables of the standard extended dataset of DB3. These have been calculated from the average of the quoted errors for each individual tokamak.

	$\ln(I)$	$\ln(n)$	$\ln(B)$	$\ln(P)$	$\ln(R)$	$\ln(A)$	$\ln(a)$	$\ln(M)$	$\lambda_e + \lambda_{pc}$	***ERR***
PC1	0.463	-0.026	0.079	0.532	0.217	0.609	0.274	0.049	1.632	0.05
PC2	0.246	0.724	0.358	0.313	-0.218	-0.317	-0.190	0.071	0.664	0.09
PC3	-0.277	-0.386	0.645	0.340	0.368	-0.307	-0.004	-0.112	0.380	0.15
PC4	**0.499**	-0.084	**0.531**	**-0.665**	0.045	0.065	0.092	0.066	0.330	**0.29**
PC5	-0.314	**0.548**	0.002	-0.243	**0.672**	0.205	0.102	-0.193	0.176	**0.28**
PC6	-0.207	0.022	0.042	-0.018	0.144	0.049	-0.021	**0.965**	0.157	**0.52**
PC7	**-0.487**	0.124	0.358	-0.040	**-0.537**	0.360	**0.445**	-0.052	0.105	**0.25**
PC8	0.143	0.050	-0.193	0.023	0.085	**-0.506**	**0.819**	0.069	0.060	**0.57**

Table 5: Principal components of the standard extended dataset of DB3 with estimates of $\lambda_e + \lambda_{pc}$ and ERR as explained in the text. Values of ERR>0.25 are shown in bold face along with the leading terms in these PCs.

[1]. Christiansen J. P., et al., Nucl. Fusion **32** (1992) 291
[2]. Thomsen K., for the ITER H-Mode Database Working Group, Nucl. Fusion **34** (1994) 131
[3]. Horton L. D., et al., Plasma Phys. Contr. Fusion **44** (2002) A273
[4]. Hubbard A., et al., Phys. Plasmas **4** (1998) 1744
[5]. Hughes J. W., et al., Rev. Sci. Instrum. **72** (2001) 1107
[6]. Hutchinson I. H., et al., Plasma Phys. Contr. Fusion **41** (1999) A609
[7]. Groebner R. J., et al., Proc. 16th Int. Conf. on Fusion Energy, Montréal, Canada, IAEA, 1 (1996) 867
[8]. Hughes J. W., et al., Phys. Plasmas **9** (2002) 3019
[9]. Fielding S. J., et al., Nucl. Fusion **41** (2001) 909
[10]. Valovi_ M., et al., Proc. of 26th EPS Conf. on Contr. Fusion and Plasma Phys., ECA 23J (1999) 149
[11]. Kardaun O. J. W. F., for the H-mode Database Working Group, "ITER: Analysis of the H-mode Confinement and Threshold Databases", Plasma Phys. and Contr. Fusion Research (Proc. 14th Int. Conf., Wüerzurg, 1992) IAEA, Vienna (1993) 251
[12]. Jackson G.L., et al., Phys. Rev. Lett. **67** (1991) 3098
[13]. Lao, L. L., et al., Nucl. Fusion **25** (1985) 1611
[14]. Lao, L. L., et al., Nucl. Fusion **30** (1990) 1035
[15]. Petty C.C., et al., Phys. Plasmas **2** (1995) 2342
[16]. Petty C.C., et al., Nucl. Fusion **38** (1998) 1183.
[17]. Petty C.C. and Luce, T.C., Phys. Plasmas **6** (1999) 909
[18]. Mahdavi A.M., et al., Plasma Phys. Contr. Fusion **21** (1997) 1113
[19]. Mahdavi A.M., et al., Nucl. Fusion **42** (2002) 52
[20]. Osborne T.H., Phys. Plasmas **8** (2001) 2017
[21]. Groebner, R.J., et al., Nucl. Fusion **41** (2001) 1789
[22]. Keilhacker M., JET Team, Plasma Phys. Contr. Fusion 37A (1995) 3
[23]. Horton L., et al., Nucl. Fusion **39** (1999) 1
[24]. Cordey J. G., et al., Plasma Phys. Contr. Fusion **44** (2002) 1929
[25]. McDonald D. C., et al., "ITER Shaping and Elongation experiments on JET", Fusion Energy 2000 (Proc. 18th Int. Conf. Sorrento, 2000). IAEA, Vienna (2001), (CD-ROM file EX2/3)
[26]. Saibene G., et al., Nucl. Fusion **39** (1999) 1133
[27]. Ongena J., et al., "Recent progress on JET towards the ITER reference Mode of operation at high density", Proc. 28th EPS Conf. on Contr. Fusion and Plasma Phys., Madeira 2001
[28]. Jacquinot J., et al., Nucl. Fusion **39** (1999) 235
[29]. Cordey J. G., et al., Nucl. Fusion **39** (1999) 301
[30]. McDonald D. C., et al., Plasma Phys. Contr. Fusion **46** (2004) 519
[31]. Greenwald M., et al., Nucl. Fusion **28** (1988) 2199
[32]. Horton L., et al., "Pellet fuelling and ELMy H-mode physics in JET", Fusion Energy 2000

(Proc. 18th Int. Conf. Sorrento, 2000). IAEA, Vienna (2001), (CD-ROM file EX2/1)
[33]. Valovic M., et al., Plasma Phys. Contr. Fusion **44** (2002) 1911
[34]. Sartori R., et al., "Confinement loss in JET ELMy H-modes", 26th EPS Conf. on Contr. Fusion and Plasma Phys., Maastricht, ECA Vol. 23J (1999) 197
[35]. Lomas P. J., for the JET team, in Fusion Energy 1996 (Proc. 16th Int. Conf. Montréal, Canada, 1996) 1, IAEA, Vienna (1997) 239
[36]. Matthews G.,et al., Nucl. Fusion **39** (1999) 19
[37]. Kadomstev B. B., Sov. J. Plasma Phys. **1** (1975) 295
[38]. Connor J. W. and Taylor J. B., Nucl. Fusion **17** (1977) 1047
[39]. Luce T. C., et al., in Fusion Energy 1996 (Proc. 16th Int. Conf. Montréal, Canada, 1996) 1, IAEA, Vienna (1997) 611
[40]. Cordey J. G., for the JET Team, in Fusion Energy 1996 (Proc. 16th Int. Conf. Montréal, Canada, 1996) 1, IAEA, Vienna (1997) 603
[41]. McDonald D. C., et al., Plasma Phys. Contr. Fusion **46** (2004) A215
[42]. McDonald D. C., et al., "Particle and energy transport in dedicated dimensionless parameter scans in JET ELMy H-modes", in preparation for Plasma Phys. Contr. Fusion
[43]. Christiansen J. P., et al., "Experimental tests of Confinement Scale Invariance on JET, DIIID, ASDEX Upgrade and CMOD", Fusion Energy 1998 (Proc. 17th Int. Conf. Yokohama, 1998). IAEA, Vienna (2001), (CD-ROM file EXP2/02)
[44]. Luce T. C., et al., Nucl. Fusion **42** (2002) 1193
[45]. Start D. F. H., et al., Phys. Rev. Lett. **80** (1998) 4681
[46]. Lingertat J., et al., J. Nucl. Mater. 266-269 (1999) 124
[47]. Rimini F., et al., "Core and Edge Confinement Studies with Different Heating Methods in JET", Fusion Energy 2000 (Proc. 18th Int. Conf. Sorrento, 2000). IAEA, Vienna (2001), (CD-ROM file EX2/6)
[48]. Asakura N., et al., Plasma Phys. Contr. Fusion **39** (1997) 1295
[49]. Shirai H., et al., Plasma Phys. Contr. Fusion **42** (2000) 1193
[50]. Fukuda T., et al., Plasma Phys. Contr. Fusion **42** (2000) A289
[51]. Urano H., et al., "Confinement degradation with beta for ELMy H-mode plasmas in the JET-60U tokamak", to be published in Nucl. Fusion
[52]. Pankin, A., et al., "The Tokamak Monte Carlo Fast Ion Module NUBEAM in the National Transport Code Collaboration Library", Computer Phys. Communications 159 (2004) 157
[53]. Akers, R. A., et al., Plasma Phys. and Contr. Fusion **45** (2003) A175
[54]. Valovic, M., et al., submitted to Nucl. Fusion
[55]. Valovic M., et al., "Energy confinement in ELMy H-modes on MAST", Proc. 29th EPS Conference, Montreux 2002, ECA 26B (2002) 1.054
[56]. Groebner R., et al., Plasma Phys. Contr. Fusion **40** (1998) 673
[57]. Maingi R., et al., Nucl. Fusion **45** (2005) 1066

[58]. Gryaznevich M., et al., Phys. Rev. Lett. **80** (1998) 3972
[59]. Sykes A., et al., Phys. Rev. Lett. **84** (2000) 495
[60]. Alikaev V.V., et al., Plasma Phys. Reports **26** (2000) 917
[61]. Esipchuk Yu. V., et al., "H-mode features under ECRH on T-10", Fusion Energy 2000 (Proc. 18th Int. Conf. Sorrento, 2000). IAEA, Vienna (2001), (CD-ROM file EXP5/16)
[62]. Khimchenko L.N.,.Krupin V.A, Timchenko N.N., 30th EPS Conference on Contr. Fusion and Plasma Phys., St. Petersburg, 7-11 July 2003 ECA Vol. 27A, P-3.119
[63]. Snipes J.A., et al., Plasma Phys. Control. Fusion **42** (2000) A299
[64]. Matsuda K., IEEE Trans. Plasma Sci. **17** (1989) 6
[65]. Pereverzev G.V., Yushmanov P.N., "ASTRA automated system for transport analysis in a tokamak", IPP Report 5/98, 2002, Max-Planck-Institut fur Plasmaphysik, Garching
[66]. ITER Physics Basis, Nucl. Fusion **39** (1999) 2175
[67]. Pacher G. W., et al., J. Nucl. Mater. 266–269 (1999) 911
[68]. Bell M. G., et al., Plasma Phys. Contr. Fusion, **28** (1986) 1329
[69]. Vorobiev G.M., et al., Plasma Phys. Rep. **9** (1983) 105
[70]. Sharapov V. M., et al., J. Nucl. Mat. 220-222 (1995) 730
[71]. Lebedev S. V., et al., Plasma Phys. Control. Fusion **36** (1994) B289
[72]. Kardaun O. J. W. F., for the International Confinement Database Working Group, "Next step tokamak physics: confinement-oriented global database analysis", Fusion Energy 2000 (Proc. 18th Int. Conf. Sorrento, 2000). IAEA, Vienna (2001), (CD-ROM file ITERP/04)
[73]. Thomsen K., et al., "Analysis of bias in H-mode confinement scaling expressions related to measurement errors in variables", to appear in Proc. of 31st EPS Conf. on Contr. Fusion and Plasma Phys., London, 2004
[74]. Cordey J. G., for the ITPA H-Mode Database Working Group, Nucl. Fusion **45** (2005) 1078
[75]. Cordey J. G., for the ITER Confinement Database and Modelling Working Group, Plasma Phys. Contr. Fusion **39** (1997) B115
[76]. Thomsen K., et al., "Latest results from the ITER H-mode confinement and threshold databases", (Proc. 17th Int. Conf., Yokohama, 1998). IAEA, Vienna (1999), (CD-ROM file ITERP1/07)
[77]. Kardaun O. J. W. F., Plasma Phys. Contr. Fusion **41** (1999) 429
[78]. Thomsen K., et al., Plasma Phys. Contr. Fusion **44** (2002) A429
[79]. Cordey J. G., for the ITPA H-Mode Database Working Group and ITPA Pedestal Database Working Group, Nucl. Fusion **43** (2003) 670
[80]. Hatae T., et al., Nucl. Fusion **41** (2001) 285
[81]. Osborne T. H., et al., "Characteristics of the H-mode pedestal and extrapolation to ITER", (Proc. 19th Int. Conf., Lyons, 2002). IAEA, Vienna (2003), (CD-ROM file IAEA-CN-94/CT-3)
[82]. Fuller W. A., 1987, "Measurement error models", New York, Wiley

[83]. The ASDEX Team, Nucl. Fusion **29** (1989) 1959
[84]. Kardaun O. J. W. F., "Interval estimate of the global energy confinement time in ITER-FEAT, based on the international multi-tokamak ITERH.DB3 dataset", IPP Internal Report IPP-IR 2002/ 1/1, available at http://www.ipp.mpg.de/ipp/netreports
[85]. Wagner F, et al., Plasma Phys. and Controlled Fusion Research (Proc. 13 Int. Conf., Washington, 1990) Vol. 1, IAEA, Vienna (1991) 277
[86]. http://v8doc.sas.com/sashtml/
[87]. Barlow R. J., "Statistics: A guide to the Use of Statistical Methods in the Physical Sciences", 1989, Chichester, John Wiley & Sons
[88]. Sivia D. S., "Data analysis: A Bayesian tutorial", 1996, Oxford, Oxford University Press
[89]. Kardaun O. J. W. F., "Classical methods of statistics with applications in fusion-oriented plasma physics", 2005, Heidelberg, Springer
[90]. Dose V., et al., Nucl. Fusion **36** (1996) 735
[91]. Kaye S. M., "The Role of Aspect Ratio and Beta in H-mode Confinement Scalings", accepted for publication in Plasma Phys. Contr. Fusion
[92]. Petty C. C., et al., Phys. Plasmas **5** (1998) 1695
[93]. Thomsen K., et al., "Confinement identity experiments in ASDEX Upgrade and JET", Proc. 25th EPS Conf. on Contr. Fusion and Plasma Phys., Prague, 1998, 468
[94]. Christiansen J. P. and Cordey J. G., Nucl. Fus. **38** (1998) 1757
[95]. Waltz R. E., et al., Phys. Rev. Lett. **65** (1990) 2390
[96]. Greenwald M., et al., Plasma Phys. Contr. Fusion **40** (1998) 789
[97]. Valovic M. for the ITPA H-Mode Database Working Group, "An analysis of the ITER H-mode confinement database", Proc. 25th EPS Conf. on Contr. Fusion and Plasma Phys., Praha,1998, ECA 22C (1998) B122
[98]. Petty C. C., et al., Phys. Plasmas **11** (2004) 2514
[99]. Takizuka T., et al., "Origin of the various beta dependence on ELMy H-mode confinement properties", submitted to Plasma Phys. Contr. Fusion.
[100]. Valovi_ M. et al., Nucl. Fusion **45** (2005) 942
[101]. Luce T. C., et al., "Application of dimensionless parameter scaling to the design and analysis of magnetic fusion experiments", in preparation for Plasma Phys. Contr. Fusion
[102]. Stober J., et al., Plasma Phys. Contr. Fusion **43** (2001) A39
[103]. Itami K., et al., Plasma Phys. Contr. Fusion **37** (1995) A255
[104]. Pochelon A., et al., Nucl. Fusion **39** (1999) 1807
[105]. Thomas P. R., et al., Phys. Rev. Lett. **80** (1998) 5548
[106]. Petty C. C., Phys. Rev. Lett. **83** (1999) 3661
[107]. Asp E., et al., Plasma Phys. Contr. Fusion **47** (2005) 505
[108]. Murakami M., et al., Proc. of the 10th International Conference on Plasma Phys. Contr. Nucl. Fusion Res., London, Vol. I, **87** (IAEA, Vienna) (1985)

[109]. Gehre O., et al., Phys. Rev. Lett. **60** (1988) 1502
[110]. Ida K., et al., Phys. Rev. Lett. **68** (1992) 2182
[111]. Miura Y., et al., Plasma Phys. Contr. Fusion **40** (1998) 799
[112]. Petty C. C., et al., Phys. Plasmas **9** (2002) 128
[113]. Counsell G. F., et al., Nucl. Fusion **45** (2005) S157
[114]. Konings J. A., et al., Nucl. Fusion **37** (1997) 199
[115]. Takizuka T., Plasma Phys. Contr. Fusion **40** (1998) 851
[116]. Coppi B. and Sharky N., Nucl. Fusion **21** (1981) 1363
[117]. Garbet X., et al., Plasma Phys. Contr. Fusion **46** (2004) 1351
[118]. Polevoi A. R., et al., J. Plasma Fusion Res. Series **5** (2002) 82
[119]. Imbeaux F., et al., Plasma Phys. Contr. Fusion **47** (2005) B179
[120]. Boucher D., for the 1D ITER Modelling Working Group, Nucl. Fusion **40** (2000) 1955
[121]. Mukhatov V., et al., Nucl. Fusion **43** (2003) 942
[122]. Kardaun O. J. W. F., et al., "On dimensionless parameters in global confinement: analysis based on ITERH.DB3/L.DB2 Database", Proc. 9th IAEA Technical Meeting on H–mode Phys. and Transport Barriers, San Diego, 2003
[123]. Strand P., et al., Nucl. Fusion **38** (1998) 545
[124]. Kinsey J. E., et al., Phys. Plasmas **12** (2005) 052503

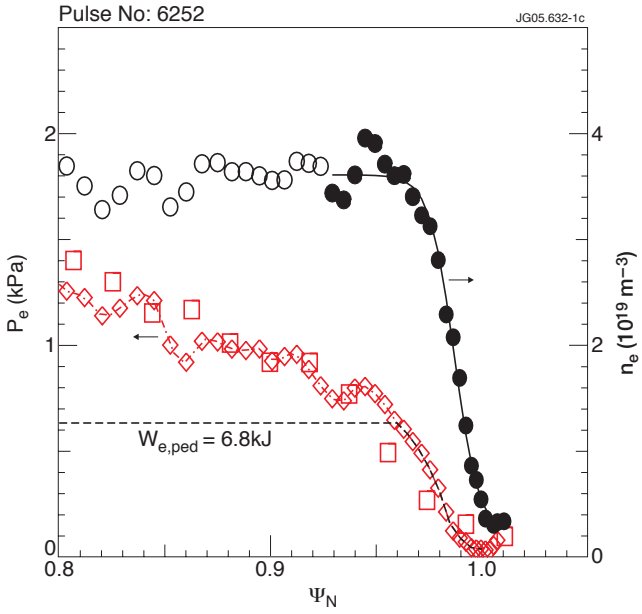

Figure 1: Evaluation of pedestal electron energy content from MAST.

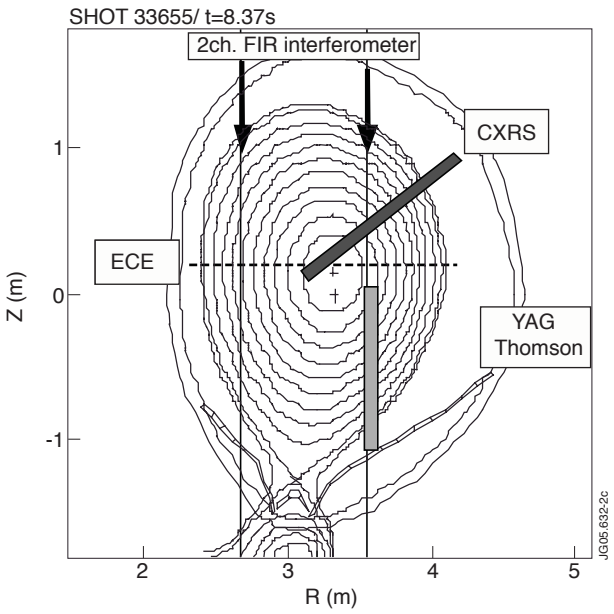

Figure 2: Plasma configuration and main diagnostics on JT-60U.

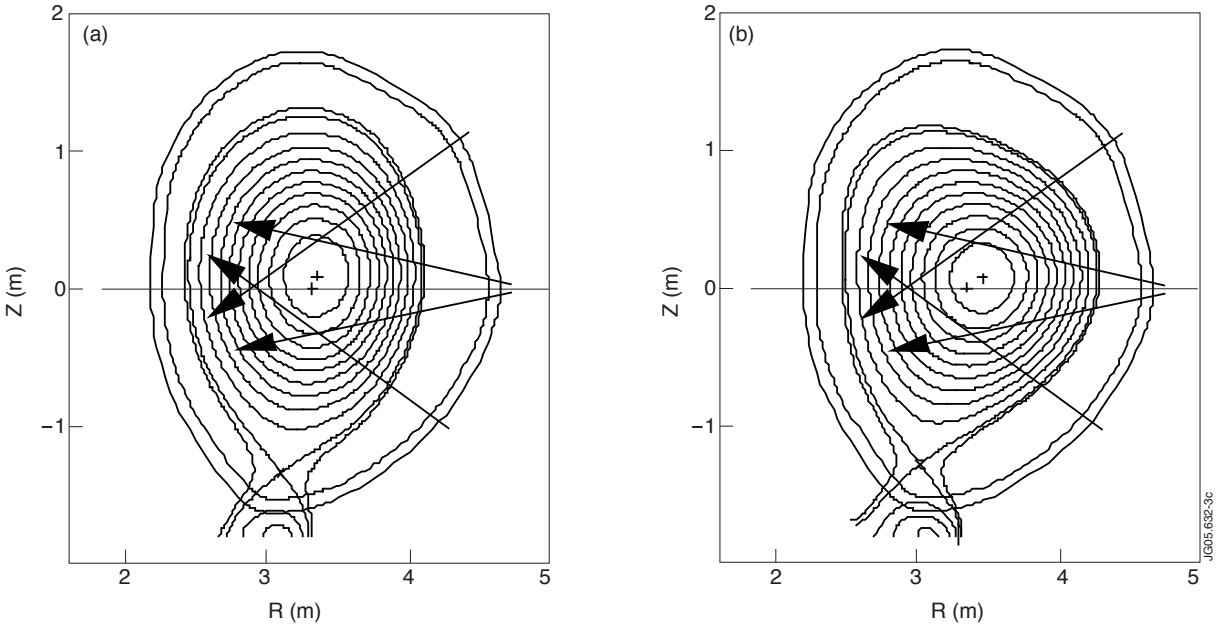

Figure 3: Plasma configurations and beam lines for a (a) low-δ and (b) high-δ discharge on JT-60U.

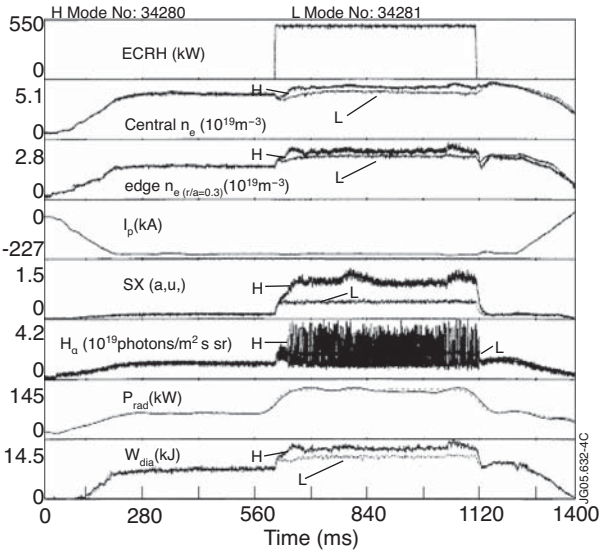

Figure 4: Time traces for main parameters in a typical H-mode discharge on TdeV.

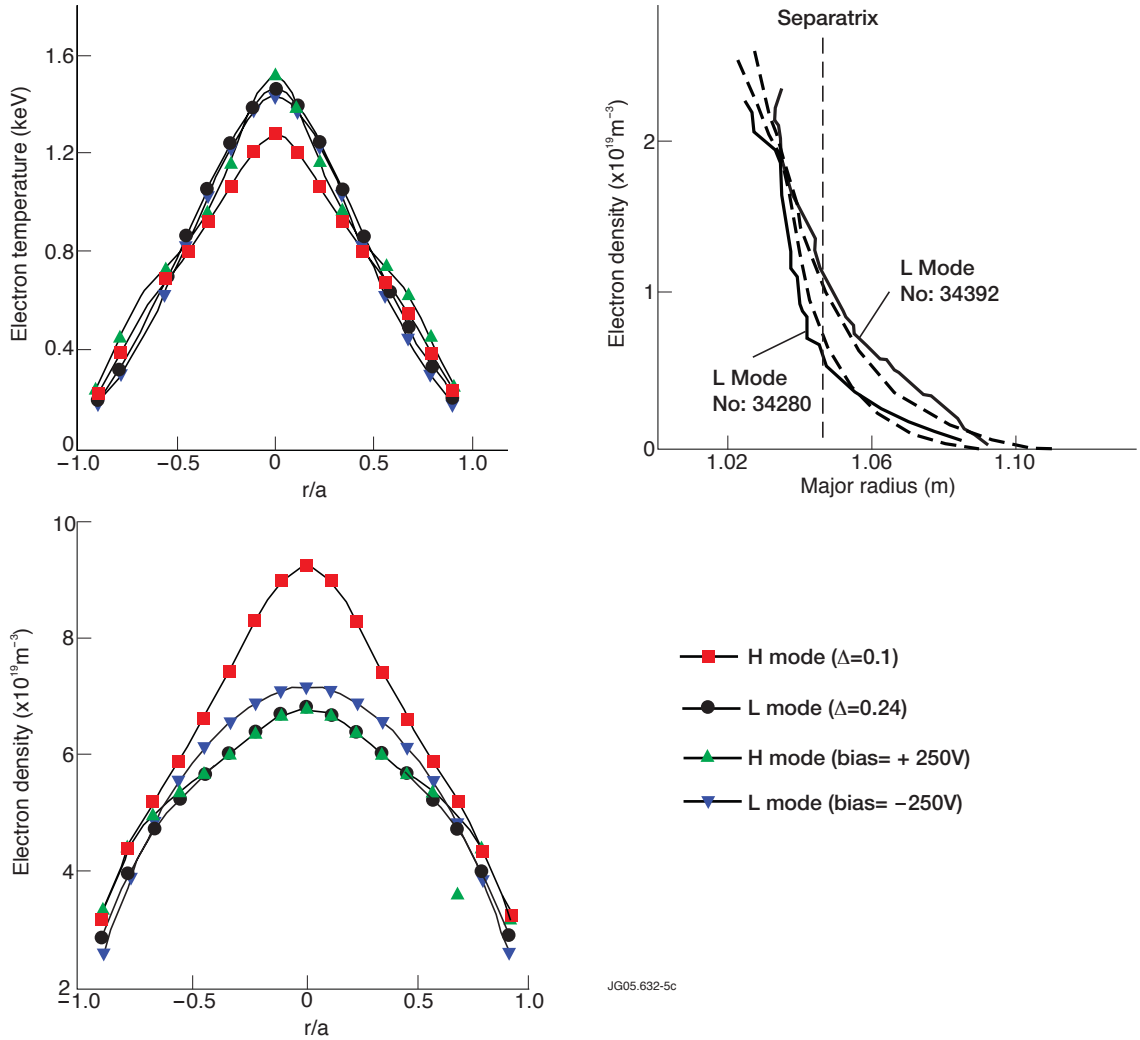

Figure 5: (a) Electron temperature and (b) density profiles measured with the interferometer and Thomson scattering diagnostics for four TdeV discharges (with a triangularity of 0.1 and 0.24 and biasing voltages of -250 and +250 V); and (c) electron density profile around the separatrix measured by the reflectometry for a H-mode and L-mode discharge (with triangularities of 0.1 and 0.24). The Δ symbol is used for triangularity.

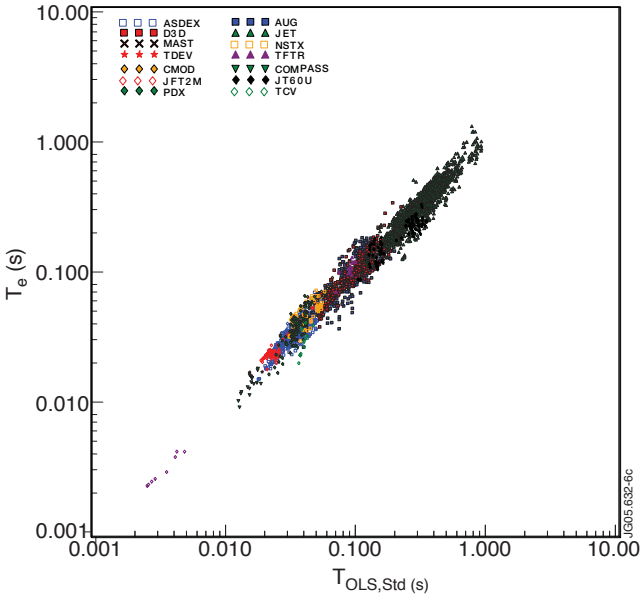

Figure 6: Comparison of the experimentally observed energy confinement time with a scaling expression derived from an OLS fit to the standard dataset, Equation 4a.

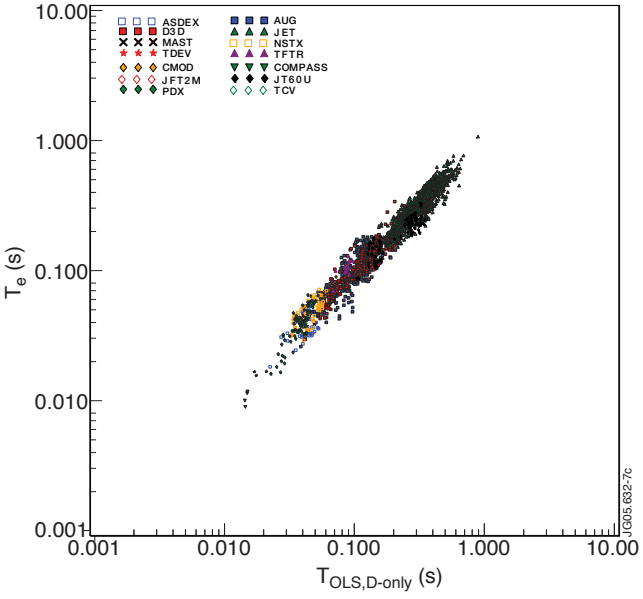

Figure 7: Comparison of the experimentally observed energy confinement time with a scaling expression derived from an OLS fit to the non-Ohmic, deuterium only dataset, Equation 4b.

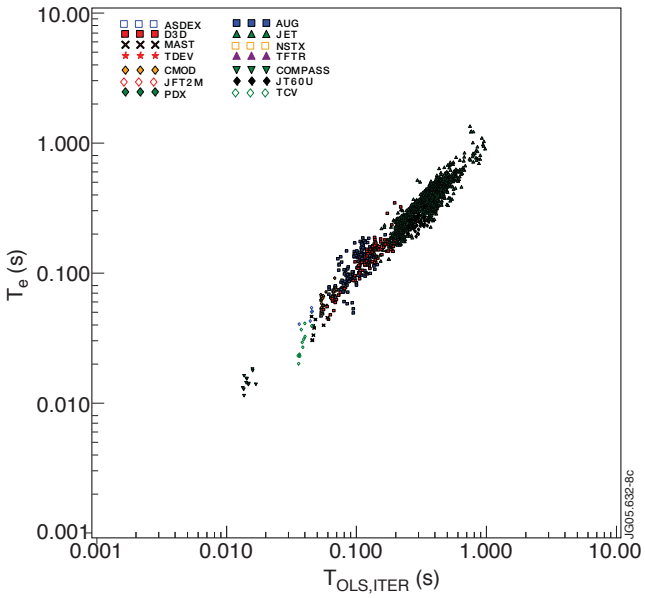

Figure 8: Comparison of the experimentally observed energy confinement time with a scaling expression derived from an OLS fit to the ITER-like dataset, Equation 4c.

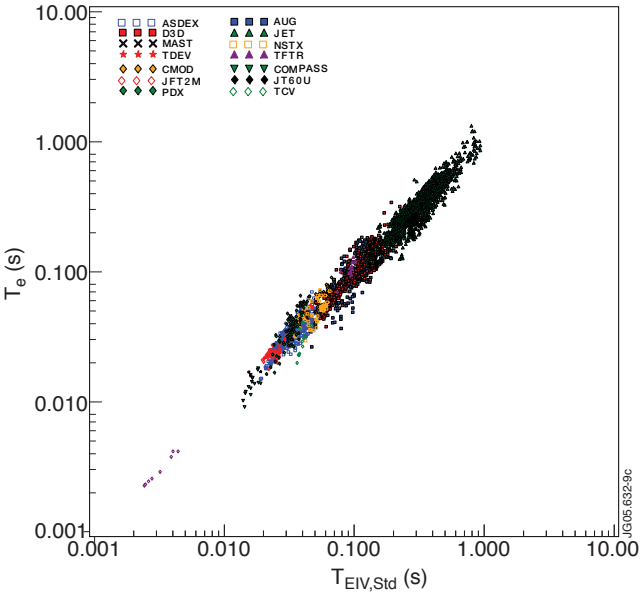

Figure 9: Comparison of the experimentally observed energy confinement time with a scaling expression derived from an EIV fit to the standard dataset, Equation 5.

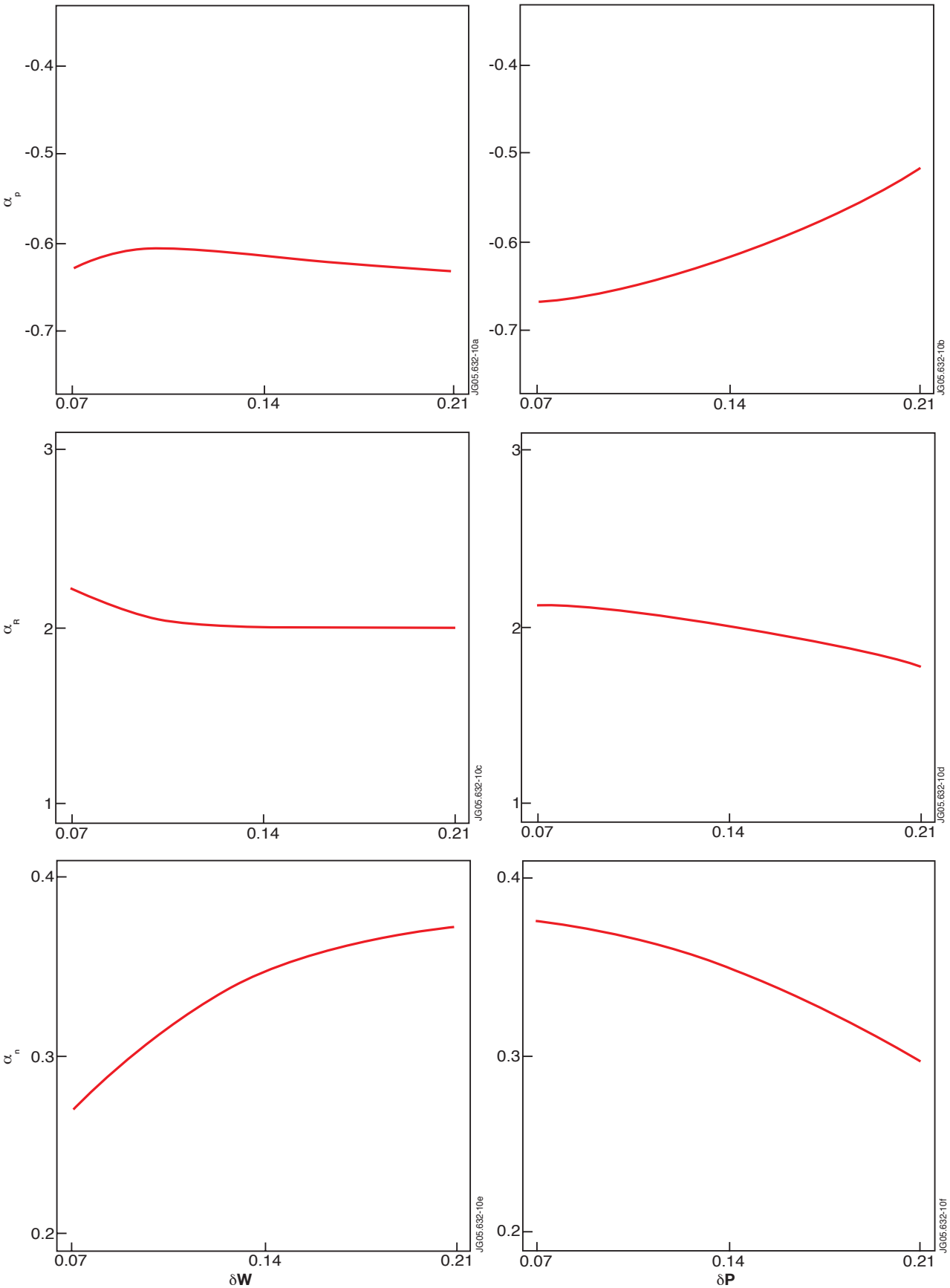

Figure 10: The variation of the exponential powers of P (α_P), (α_R), and n (α_n) with the errors in P and W_{th} resulting from an Errors in Variables fit to the standard set. The errors in the other parameters are fixed at the values given in Table 4.

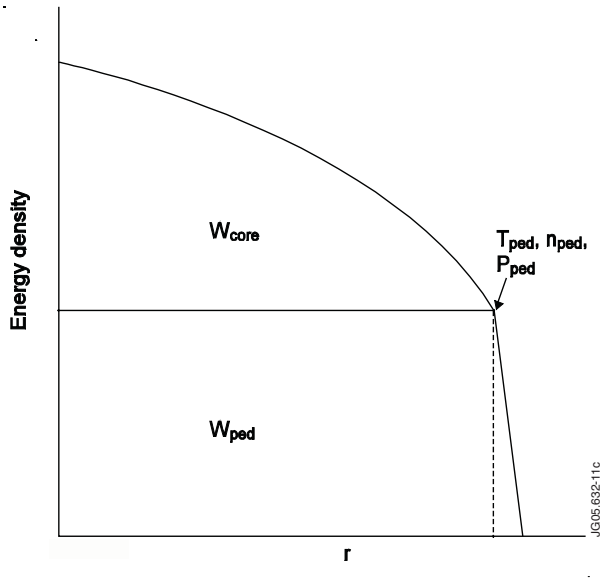

Figure 11: Schematic diagram of the energy density versus radius. The energy in the pedestal W_{ped} and W_{core} the core are marked.

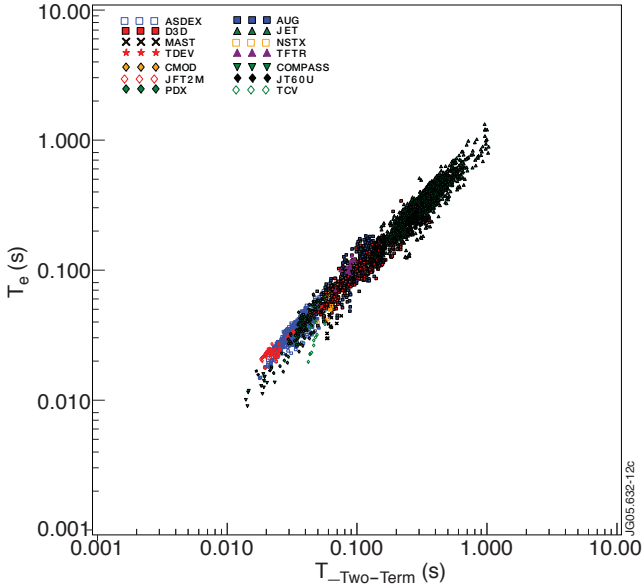

Figure 12: Comparison of the experimentally observed energy confinement time with a scaling expression derived from a two-term fit.

	$\ln(I)$	$\ln(n)$	$\ln(B)$	$\ln(P)$	$\ln(R)$	$\ln(A)$	$\ln(a)$	$\lambda_e + \lambda_{pc}$	***ERR***
PC1	0.423	-0.117	0.037	0.493	0.254	0.638	0.303	1.345	0.03
PC2	0.322	0.712	0.381	0.359	-0.194	-0.237	-0.146	0.687	0.10
PC3	-0.025	-0.488	0.768	0.112	0.262	-0.300	-0.018	0.344	0.33
PC4	0.542	0.063	0.266	-0.756	-0.074	0.179	0.151	0.310	0.13
PC5	-0.316	0.459	0.087	-0.202	0.792	0.118	0.024	0.156	0.28
PC6	-0.561	0.155	0.393	-0.036	-0.436	0.384	0.409	0.105	0.60
PC7	0.089	0.055	-0.174	0.046	0.084	-0.503	0.834	0.059	0.62

Table 6: Principal components of the non-Ohmic, deuterium only dataset of DB3 with estimates of $\lambda_e + \lambda_{pc}$ and ERR as explained in the text.

	$\ln(\boldsymbol{I})$	$\ln(\boldsymbol{n})$	$\ln(\boldsymbol{P})$	$\ln(\boldsymbol{R})$	$\ln(\boldsymbol{a})$	$\lambda_e + \lambda_{pc}$	***ERR***
PC1	0.467	-0.131	0.729	0.347	0.336	1.194	0.074
PC2	0.079	0.852	0.353	-0.269	-0.266	0.600	0.11
PC3	0.800	0.203	-0.550	0.038	0.120	0.262	0.259
PC4	-0.322	0.435	-0.200	0.779	0.245	0.162	0.233
PC5	-0.178	0.162	-0.042	-0.445	0.861	0.099	0.247

Table 7: Principal components of the ITER-like dataset of DB3 with estimates of $\lambda_e + \lambda_{pc}$ and ERR as explained in the text.

	$\ln(I)$	$\ln(n)$	$\ln(P)$	$\ln(R)$	$\ln(a)$	$\ln(\kappa_a)$	$\ln(B)$	$\ln(M)$	$\ln(F_q)$	$\lambda_e + \lambda_{pc}$	**ERR**
PC1	0.501	-0.049	0.623	0.374	0.264	-0.023	0.365	0.047	-0.111	0.603	0.15
PC2	0.116	0.917	0.155	-0.258	-0.177	0.115	0.099	0.037	0.014	0.352	0.15
PC3	0.483	-0.012	0.058	-0.178	0.302	0.109	-0.683	0.086	0.392	0.244	0.09
PC4	0.567	0.049	-0.734	0.051	0.098	0.006	0.301	0.119	-0.144	0.171	0.61
PC5	0.068	-0.327	0.148	-0.575	-0.200	0.227	0.373	0.491	0.255	0.101	0.52
PC6	-0.286	0.181	-0.059	0.317	0.258	-0.121	-0.121	0.827	-0.047	0.077	0.93
PC7	-0.262	0.112	-0.137	0.183	0.441	0.334	0.342	-0.197	0.636	0.046	0.84
PC8	-0.085	-0.043	0.013	-0.035	0.200	0.818	-0.125	0.004	-0.515	0.030	1.38
PC9	0.138	-0.032	-0.030	0.542	-0.676	0.358	-0.115	0.107	0.276	0.021	1.71

Table 8: Principal components of the pedestal-global confinement dataset with 9 variables. Estimates of $\lambda_e + \lambda_{pc}$ and ERR as explained in the text.

	$\ln(\boldsymbol{I})$	$\ln(\boldsymbol{n})$	$\ln(\boldsymbol{P})$	$\ln(\boldsymbol{R})$	$\ln(\boldsymbol{a})$	$\lambda_e + \lambda_{pc}$	***ERR***
PC1	0.479	0.035	0.730	0.423	0.239	0.591	0.15
PC2	-0.084	0.956	0.152	-0.138	-0.191	0.286	0.21
PC3	0.659	0.240	-0.623	0.126	0.323	0.151	0.51
PC4	-0.322	0.095	-0.237	0.886	-0.215	0.096	0.33
PC5	-0.475	0.135	0.005	0.026	0.869	0.048	0.48

Table 9: Principal components of the pedestal-global confinement dataset with 5 variables. Estimates of $\lambda_e + \lambda_{pc}$ and ERR as explained in the text.

	Standard dataset	Non-Ohmic, D only dataset	ITER-like dataset
ASDEX	1/8	1/4	-
ASDEX Upgrade	1/8	1/8	1/6
C-Mod	1/4	1/4	1/4
COMPASS-D	1/3	1/3	1/3
DIII-D	1/7	1/7	1/6
JET	1/12	1/12	1/12
JFT-2M	1/5	-	-
JT60-U	1/5	1/5	1/4
MAST	1/3	1/3	1/3
NSTX	1/3	1/3	1/3
PBXM	1/4	1/4	-
PDX	1/5	1/5	-
START	1/3	-	-
TCV	1/3	-	1/3
TDEV	1/3	1/3	-
TFTR	1/3	1/3	-

Table 10: Weighting factors used for data from each tokomak in the OLS fits of Section 4.1.

	$\ln(I)$	$\ln(n)$	$\ln(P)$	$\ln(R)$	$\ln(a)$	$\lambda_e + \lambda_{pc}$	***ERR***
PC1	0.479	0.035	0.730	0.423	0.239	0.591	0.15
PC2	-0.084	0.956	0.152	-0.138	-0.191	0.286	0.21
PC3	0.659	0.240	-0.623	0.126	0.323	0.151	0.51
PC4	-0.322	0.095	-0.237	0.886	-0.215	0.096	0.33
PC5	-0.475	0.135	0.005	0.026	0.869	0.048	0.48

Table 11: Principal components of the ITER-like pedestal-global confinement dataset with estimates of $\lambda_e + \lambda_{pc}$ and ERR as explained in the text.

Equation	Scaling	$\tau_{E,ITER}$ (s)
15a	IPB98(y,2)	3.66
15b	EIV, 8 variable fit to standard DB3 dataset	3.29
15c	Two-term, five variable fit to ITER-like pedestal-global confinement DB3 dataset	3.90

Table 12: The energy confinement time, calculated from the recommended scalings of Section 6.1, for the ITER relevant parameters $\boldsymbol{I} = 15$ MA, $\boldsymbol{B} = 5.3$ T, $\boldsymbol{n} = 1.03 \times 10^{20}$ ·m-3, $\boldsymbol{P} = 87$ MW, $\boldsymbol{R} = 6.2$ m, $\boldsymbol{a} = 2.0$ m, and $\kappa_a = 1.75$. The first two scalings apply to a deuterium-tritium plasma, the third to a pure deuterium one.

Category	No.	Variables	Comments
Renames	2	UPDATE, PECH	Renamed as LCUPDATE, PECRHC
Selection markers	12	SELDB3, SELDB3X, DB2P5, DB2P8, DB3IS, DB3V5, IAEA92, IAE2000N, IAE2000X, DB3DONLY, IAE2004S, IAE2004I	
Scaling laws	11	H89, H93, HITER92Y, HITER96L, HEPS97, HIPB98Y, HIPB98Y1, HIPB98Y2, HIPB98Y3, HIPB98Y4, HMWS2003	
Book keeping	4	T1, T2, TIME_ID, TOK_ID,	
RF heating	6	ICFORM, PECRH, PICRHC, WFANIIC, WFICFORM, WFICRHP	
ELMs	5	ELMDUR, ELMFREQ, ELMINT, ELMMAX, ELMTYPE	
Rotation	5	SPIN, TORQ, VTOR0, VTORIMP, VTORV	TEXTOR only (not in H-mode set).
Shape	4	DELTAL, DELTAU, KAPPAA, KAREA	
Gas fuelling	3	FUELRATE, XGASA, XGASZ	Fuelling and impurities affect τ_E. High fuelling (based on a machine dependent criteria) and impurity discharges are removed in standard fits (including here).

Divertor	1	DIVNAME	ASDEX, ASDEX-Upgrade, DIII-D and JET have all contributed multi-divertor data
α -heating	1	PALPHA	Reflects DT work
q -profile	1	SH95	Q95 already in DB2
Nett gain	**53**		**Changes not included**

Table 13: Summary of variables in DB3 which have been added or renamed since DB2